RECENT RESULTS OF THE ACO STORAGE RING F.E.L. EXPERIMENT

M. Billardon, D. Deacon, P. Elleaume, J. Ortega, K. Robinson, C. Bazin, M. Bergher, J. Madey, Y. Petroff, M. Velghe

HAL Id: jpa-00222532
https://hal.science/jpa-00222532

RECENT RESULTS OF THE ACO STORAGE RING F.E.L. EXPERIMENT

M. Billardon[a], D.A.G. Deacon[b], P. Elleaume[c], J.M. Ortega[a],
K.E. Robinson[d], C. Bazin, M. Bergher, J.M.J. Madey[d], Y. Petroff and
M. Velghe[e]

L.U.R.E., Bât. 209C, Université de Paris-Sud, 91405 Orsay, France

(a) *Ecole Supérieure de Physique et Chimie, 10 rue Vauquelin, 75231 Paris
Cedex 05, France*
(b) *Deacon Research, 3790 El Camino Real, n° 162, Palo Alto, CA 94306, U.S.A.*
(c) *Département de Physico-Chimie, Service de Photophysique, CEN Saclay, 91191
Gif-sur-Yvette, France*
(d) *High Energy Physics Laboratory, Stanford University, Stanford, CA 94305,
U.S.A.*
(e) *Laboratoire de Photophysique Moléculaire, Bât. 213, Université de Paris-Sud,
91405 Orsay, France*

Résumé ~ Un onduleur à aimants permanents a été construit et installé sur
l'anneau de stockage ACO. La conception de cet onduleur, l'émission spontanée
et le gain du système sont présentés ici, ainsi que l'allongement du paquet
d'électron dû à un laser extérieur se propageant dans l'onduleur. Une cavité
optique a également été construite et installée sur l'anneau. Les performances
et les problèmes de dégradation des miroirs qui la composent sont discutés.
On reporte également l'observation de l'amplification de l'émission spontanée
stockée dans la cavité. Enfin, les premiers résultats obtenus sur l'émission
spontanée de l'onduleur transformé en "Klystron Optique" sont détaillés et
interprétés.

Abstract - A permanent magnet undulator has been built and installed on the ACO
Storage Ring. The undulator design, the spontaneous emission and gain of the
system, as well as the laser induced bunch lengthening of the electron bunch,
are presented. A low-loss optical cavity has been also recently built and opera-
ted on the ring. Its performance and the degradation problems of the mirrors are
discussed. Amplification of the spontaneous emission stored in the optical cavity
has been observed. Also, preliminary results on the operation of an optical
klystron are reported and interpreted.

I - INTRODUCTION

Synchrotron radiation has proved to be an extraordinarily useful source for spectros-
copic studies, materials analysis, microscopy and lithography. The impact has been
particularly strong in the short-wavelength region ($h\nu$ > 10 eV), where the spectral
brightness of synchrotron radiation is typically order of magnitude larger than that
obtainable from other light sources.

Yet it is apparent that for high-resolution studies, or studies of phenomenon invol-
ving low cross-sections, even higher spectral brightness would be desirable. The
possible means to secure this additional brightness include the use of magnetic un-
dulators as spontaneous radiation sources, or (in conjunction with a suitable opti-
cal resonator) as Free Electron Lasers.

At the present time the prospects for undulators look quite strong, and there is a

growing consensus that the next generation of synchrotron radiation sources will be based primarily on undulator and multipole wiggler radiation as compared to the existing machines which use primarily the broad-band radiation emitted by the electrons in the normal bending magnets of the ring.

Though technically more demanding , the realization of short-wavelength free-electron laser operation could raise the spectral power density available from an undulator by several additional orders of magnitude. This prospect has encouraged us to examine the problems associated with the operation of storage ring Free Electron Lasers, and to establish an experimental program to secure data on the operation of a visible-wavelength system. The choice of the visible wavelength region for the initial experiments was based on the fact that very high quality mirrors exist in this range. Very good mirrors are necessary for the operation since the straight section length in ACO is very short, and hence the gain is very small.

This study, conducted as a collaboration by LURE and Stanford using the ACO ring at Orsay, began in 1979. Although the interaction length and current density available at ACO limit the experiment to low gain, the availability factor of the machine has been good, and it has proved an excellent test-bed for the basic physics and technology issues for the FEL. In a first step, a superconducting undulator was built and installed on the storage ring ; several studies were conducted. The spontaneous emission of the system was observed / 1 / and the relationship of the spectral shape to the undulator imperfections and the beam alignment problems was clarified / 2,5 /. The optical gain as a function of the electron energy / 3,4 / and the laser induced lengthening of the electron bunch were also measured. These results have been reported at the 1981 Sun-Valley meeting / 5 /.

The second step consisted in the construction of a permanent magnet undulator/optical klystron which would be optimized at 240 MeV, the injection energy of ACO. The goal was to eliminate all the problems encountered with the operation of the superconducting undulator / 5 /. This new undulator has now been on operation for nine months, and its spontaneous emission and gain have been studied in details. A high-quality optical cavity has been mounted and operated and the amplification of the spontaneous emission has been observed. A dispersive section has been constructed and installed to convert the undulator into an optical klystron and the spontaneous emission measurements of the klystron are presented here.

Section II of this article is devoted to the problem of the design and optimization of the permanent magnet undulator. The spontaneous emission measurements, particularly in the VUV spectral range, and the gain measurements are also described. In section III are reported the new bunch lengthening measurements, the electron bunch being heated either by an external laser or by the spontaneous emission stored in the optical cavity. The first experiments with the optical klystron are discussed in section IV. The cavity Q measurements of the high quality optical cavity ($Q > 10^3$) are discussed in section V along with the problems of mirrors degradation and regeneration. Finally the cavity experiments, alignement of the cavity axis on the electron beam and first observations of the gain on the stored spontaneous radiation, are described in section VI.

II - DESIGN AND OPERATION OF THE UNDULATOR

Our new undulator which we have named N.O.E.L. (Nouvel Onduleur pour l'Etude du Laser), has been designed / 6 / with permanent magnets in order to avoid the technical problems encountered with the previous superconducting undulator / 5 /, and to achieve a higher optical gain. The design energy is 240 MeV, the injection energy of the ACO storage ring.

Design of the undulator

The magnet structure is the now classical arrangement defined by Halbach / 7 / (fig. 1). The undulator length, 1.3 m, is the maximum length available on the ACO straight section. A new beam vacuum chamber allowed us a minimum gap of 33 mm. We have chosen to work at the maximum of the gain K ≃ 2 which implied (with magnets

having a remanent field of 0.8 Tesla) a magnetic period of 78 mm. These characteristics are summarized in Table 1.

In this configuration the maximum field available B_O, is given by

$$B_O \text{ (Tesla)} = 1.426 \, B_r \, e^{-\pi g/\lambda_o} \tag{1}$$

with B_r the remanent field (0.85 T in our case), g the undulator gap and λ_o the period.

<div align="center">

Table 1

Characteristics of NOEL

</div>

Full length	1.33 m
Number of periods	17
Period	78 mm
Transverse pole width	100 mm
Vacuum chamber full gap	25 mm
Minimum undulator gap	33 mm
Maximum field	3100 Gauss
Max. Emitted Wavelength (240 MeV) ...	6400 Å
Electron Energy in ACO	150-536 MeV

The electron trajectory is adjustable by two half poles located at each end of the undulator (fig. 1). They are movable independently of the rest of the undulator in order to adjust the electron trajectory. The undulator gap is continuously adjustable from 33 to 300 mm (open position). The ring is injected with the undulator opened.

The undulator is divided into three parts comprising respectively 7, 3 and 7 periods. The central part is removable and can be replaced by a so-called "dispersive section" which will be described in section IV. The dispersive section transforms the undulator into an optical klystron /̄ 8,9 ̄/ in order to enhance the gain of the system. Its length has been chosen from the calculations described in section IV.
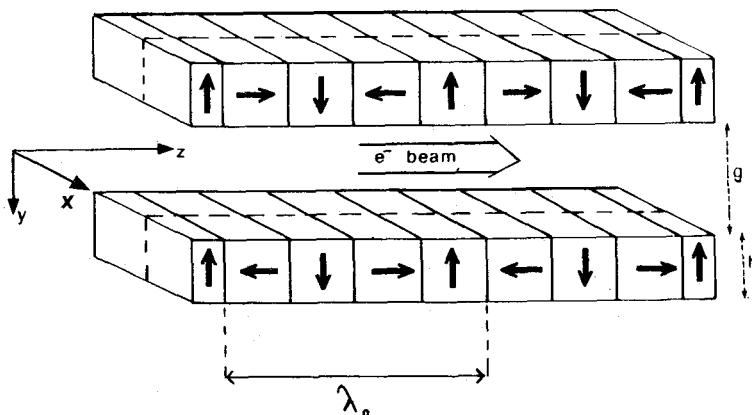

Fig. 1 - The permanent magnet undulator suggested by K. Halbach /̄ 7 ̄/ uses a configuration of magnets rotated by π/2 from one position to the following along the undulator. In this sketch of a 2 periods undulator the first and last magnets are (adjustable) half-poles. The axis convention used in this article is also shown.
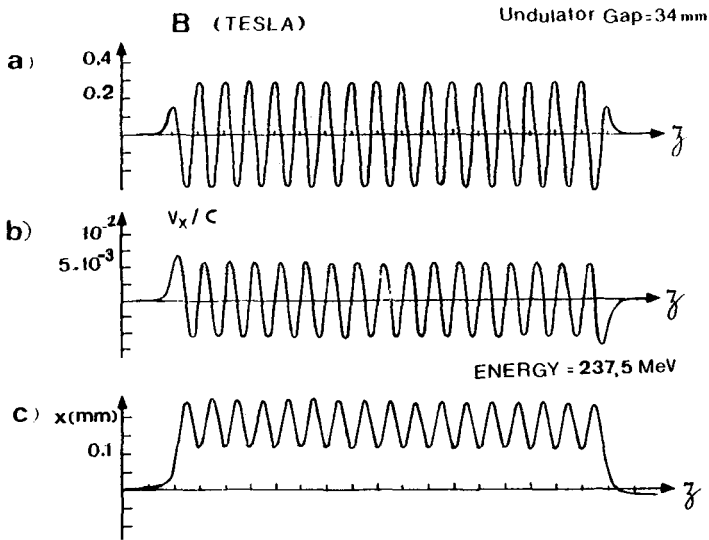
B (TESLA)   Undulator Gap=34 mm

Fig. 2 - Numerical simulation of the "perfect" undulator :

a) Magnetic field
b) Transverse speed (see eq. 2 in text)
c) Trajectory of the electron in the (xz) plane. The x component is magnified
   by 100 with respect to the z component.

The magnetic field produced along the undulator and the trajectory in the (xy) plane
of an electron traveling along this axis have been computed numerically (fig. 1).
The magnets were represented by two "charged" surfaces, the density of charge being
σ = B_r /̄ 6 /̄. The trajectory was calculated by integrating the Lorentz equations
of motion in the limit $(V_x/c)^2$ << 1. The result is shown in fig. 2. The use of half-
poles at each end on the undulator allows the adjustment of the transverse velocity
and deviation to zero at the output of the undulator so that the mean trajectory
is parallel to the undulator axis. Each of the 3 undulators (of 7, 3 and 7 periods)
composing the main undulator has been terminated by half poles so that removing the
central section to insert the klystron leaves the output speed and angle equal to
zero.

Technical construction

The 50 x 19 x 19 mm individual magnets have first been paired to form 100 mm long
magnets in the transverse direction (cf. Table 1). The resulting pairs were glued
on individual holders and clamped on benches (fig. 3a), one bench for each undula-
tor of 3 or 7 periods. The benches are attached on 1.3 m rails which are moved ver-
tically like a pair of jaws by variable speed D.C. motor (fig. 3b). The vacuum cham-
ber design also appears on fig. 3b.

We have compensated the undulator for the individual magnet block defects by selec-
ting the magnet emplacement along the undulator as a function of the individual ma-
gnet characteristics /̄ 10 /̄. This compensation has been made in 3 steps :

        - measurement of the individual blocks has shown that the remanent fields
varied from block to block (by ± 2 % FWHM) and that this field was not exactly paral-
lel to the mechanical face of the pieces (± 2 % FWHM). Each block was measured and
characterized by the value of the field on two points A and B (fig. 4). The combined
effects of the field and angle dispersions induced a total field dispersion at the
points A and B of ± 7 % FWHM (± 10 % maximum).

Figure 3 a

View of the end of the undulator,
closed on the beam vacuum chamber.
The magnets of the lower bench are
hidden by the vacuum chamber edge.
The magnets holders (in grey) are
clamped on benches (in black) which
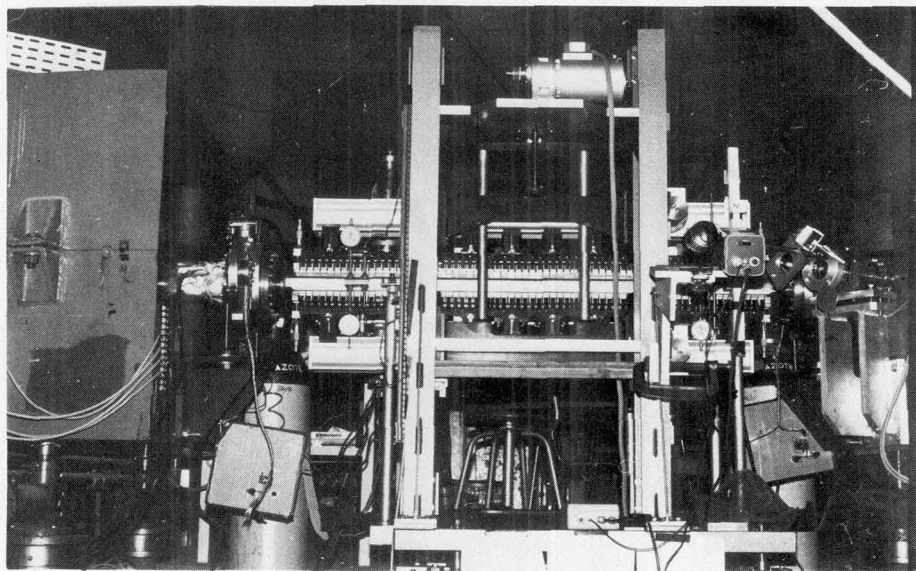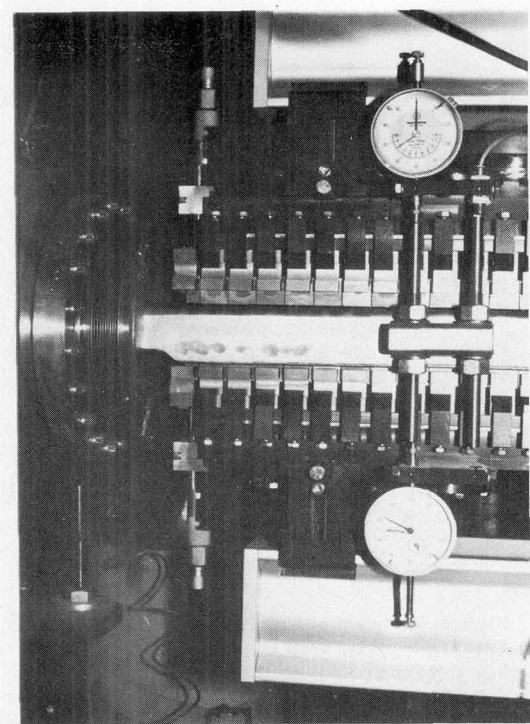may slide along aluminium rails
(in white)

Figure 3 b

General view of the undulator installed in the ACO experimental straight
section

Figure 4 – All the magnets of the undulator have been characterized by a measure of the vertical field B_y produced on the points A and B. Then the magnets with nearly identical "A" and "B" were paired in order to cancel the x-contribution of the field. The resulting pairs produce then at points A and B fields which are exactly two times the field previously measured at the same points.
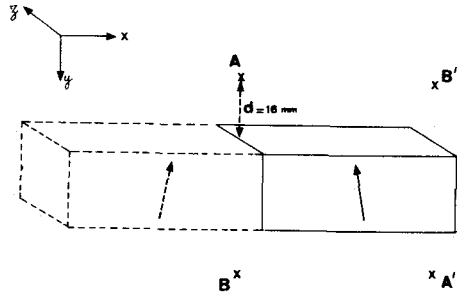
Figure 5 – Magnetic measurements of the vertical field B_y, produced by the undulator on its axis

-a- Magnetic field

-b- Simulation of the electron trajectory in the x-z plane

Figure 6 – Spontaneous emission spectrum of the light emitted in the forward direction by 237.5 MeV electrons.

xxx Theoretical spectrum (from the field simulation of fig. 2 of a "perfect" undulator)

ooo Spectrum calculated from the magnetic measurement data obtained from the "real"undulator

—— Experimental spectrum taken with the undulator placed on the ACO storage ring

– the blocks were paired so that the angular orientation of the field be compensated, at least for the transverse (B_x) component of the field (fig. 4).
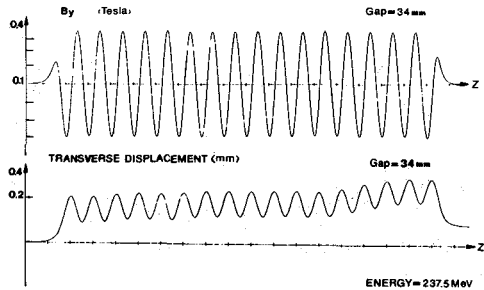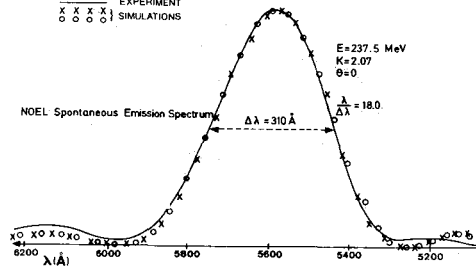
– the pairs have been placed along the undulator so that each "vertical" magnet (magnetization perpendicular to the electron beam direction) has its on-axis remanent field value close to the average and is surrounded by horizontal magnets offering on one side a weaker-than-average face and on the other side a stronger-than-average face. The blocks have been chosen graphically (in the graph drawn with the magnetic measurements) so that the center of gravity of the field produced by each period remains approximatively constant. For more details, see reference /¯10_/.

Magnetic measurements

Magnetic measurements have been carried out along the undulator axis with a Hall probe driven by a stepping motor. The output of the probe was digitized and the electron trajectory inside the undulator was calculated in real time (fig. 5) using the equations

$$V_x(z) = \frac{e}{\gamma m} \int_0^z B_y(1) \, dl$$

$$x(z) = \frac{1}{c} \int_0^z V_x(u) \, du \qquad\qquad (2)$$

where V_x and x are the transverse speed and deviation of the electron in the undulator.

This experiment allowed us to adjust the half poles located at each end of the undulator so that the output transverse deviation and speed remain within tolerance over the range of undulator gaps between 33 and 50mm. From these results the displacement of the closed orbit of the storage ring in the undulator as a function of the gap can be calculated from the optics of the machine /¯10,11_/. We have found that for a typical 5 mm gap scan the position and angle of the beam varied by 43 μm and 15 μrad, respectively. These values are compatible with gain measurements where the probe laser beam transverse section area is of the order of 0.5 mm² and where the gap is scanned over a few millimeters during the experiment.

The success of our optimization method is demonstrated by the measured field amplitude dispersion which is less than ± 1 %, except for the first and last oscillations for which the end effects cause a deviation (fig. 2). We have also measured the B_x and B_z field and found that they are smaller than 1 % of the main (B_y) field.

The power spectrum emitted by the electrons has also been simulated using the Lienard-Wiechert formula /¯12_/ :

$$\frac{dW}{d\Omega d\omega} = \frac{e^2 \omega^2}{4\pi^2 c} \left| \int_{-\infty}^{+\infty} \vec{n} \wedge (\vec{n} \wedge \vec{\beta}) \, e^{i\omega(t - \frac{\vec{n}\vec{r}}{c})} \, dt \right|^2 \qquad\qquad (3)$$

where $\vec{n}$ is the unit vector in the direction of observation and $\vec{r}$ the electron trajectory. The integration has been done numerically by transforming the integration on t to an integration on z (forward direction) in the limit $\gamma \gg 1$ and $\beta_x \ll 1$ which is obvious good in our case (E ≃ 240 MeV, K ≃ 2). The result is shown on fig. 6 and compared with the theoretical spectrum computed from the numerical simulation of a perfect undulator shown on fig. 1. The B_x field has been introduced into the numerical simulations and its effect on the shape of the curve, has been found to be negligible. The result is very satisfactorily and shows that our opti-
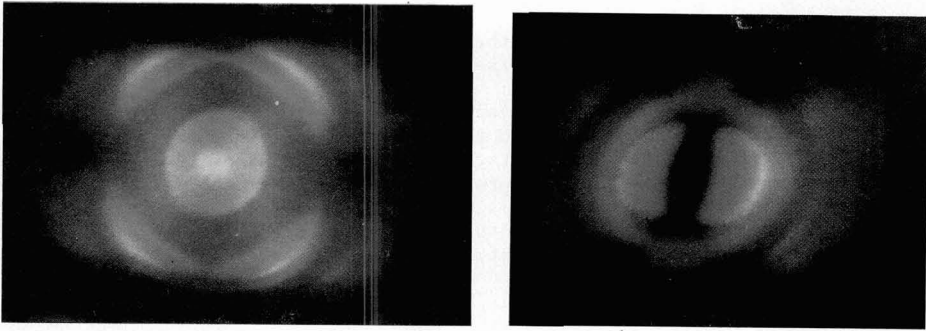
Figure 7 - Pictures of the spontaneous emission of the undulator
-a- at 237.5 MeV the wavelength of the first harmonic at the center is, for K=2.15,
    λ_1 = 597 nm
-b- at 150 MeV and K = 1.86 the wavelength emitted at the center are : λ_1 = 1100 nm
    (Infra-red), λ_2 = 505 nm and λ_3 = 336 nm (Ultra-violet). Since the intensity
    of the 2nd harmonic is nul in the forward direction, the center of the picture
    looks black.

Figure 8

a Ring profiles of the
  first harmonic in
  the vertical and
  horizontal directions

b Spectral distribution
  of the light emitted in
  the 3rd and 5th harmonic
  (at low energy) in the
  forward direction ($\Theta = 0$)

mization method has prevented trajectory distortions from broadening the spectral width of the spontaneous emission and diminished the optical gain (the loss on the gain was about 50 % with our previous superconducting undulator / 6 7).

Spontaneous emission

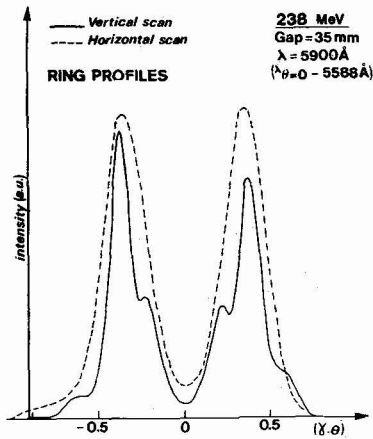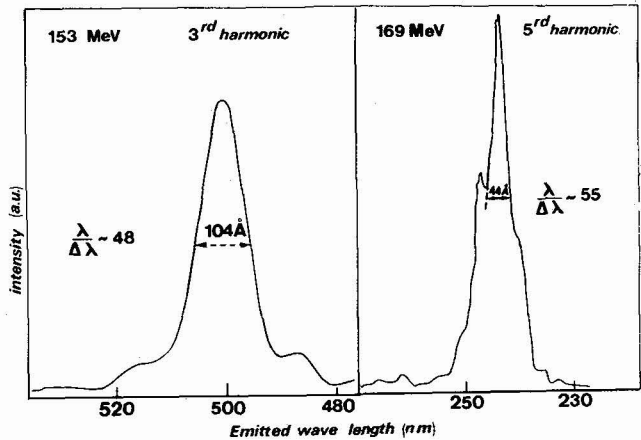The ACO storage ring is injected with the undulator in the open position. When the electron current is established the undulator is closed down and the storage ring tunes are adjusted, to take into account the quadrupolar focussing effect introduced by the undulator / 11, 13 7 . However the beam lifetimes drops considerably by a factor of 2 to 3, when the undulator is closed. This effect is not yet understood.

The electron beam is aligned with the undulator axis by an optical technique. A white light beam is sent, from outside the ring, through the undulator vacuum chamber. With a telephoto lens system an optical image is made of either the beginning or the end of the undulator. The electron beam appears as a brilliant spot, within the image of the edges of the vacuum chamber. The electron beam position is then be adjusted with the storage ring horizontal and vertical correction coils. The accuracy of the adjustment is $\pm$ 1 mm which is satisfactory, given the field homogeneity in the undulator.

The spontaneous emission of the undulator looks, as usual / 1,5 7 like a series of concentric coloured rings (fig. 7), the different harmonics of the fundamental frequency being visible successively from the center toward the exterior. The dark spots in the radiation pattern at 237 MeV are due to the dipole-like character of the emission. The photograph taken at 150 MeV of the second harmonic is dark at the center since the even harmonics have a zero intensity in the forward direction / 1 7.

The spectral distribution of the first harmonic of the emitted radiation at the center of the rings is shown on fig. 6. It agrees well with the theory and magnetic simulation except in the wings of the distribution. The distorsion of the wings of the curves appears to be due to the residual horizontal field produced by the bending magnets of the ring with is still about 100 Gauss at the entry of the undulator. The space between the magnet iron and the undulator is only 25 cm long. However the small discrepancies with the theoretical spectrum should not affect the optical gain, which is proportional to the derivative of that curve / 3, 14 7. The ring profiles have also been measured in the vertical and horizontal direction (fig. 8a). In this experiment a pinhole is moved in a transverse direction, the monochromator being set at a fixed wavelength corresponding to the wavelength of the desired ring. The ring profile is quite symmetric with respect to the center in the horizontal direction although in the vertical direction there is a difference of about 20 % between the two peaks. This last effect could be produced by the residual B_x field in the undulator / 10 7 which bends the electron beam trajectory in the vertical plane, leading to asymmetry in that plane ; despite the fact that this field has been reduced to less than 1 % of the main field by our compensation method.

Several harmonics of the fundamental frequency have been observed in the visible spectral region at low energy (fig. 8b). The homogeneous theoretical spectral width of the harmonics is 1/nN if N is the number of periods of the undulator and n the harmonic number. The 1st and 3rd harmonic have the theoretical width although the higher ones are distorted and their relative widths are limited to about 1/55, due to the residual undulator imperfections,the residual bending magnets field and to the angular divergence of the electron beam.

The emission of the undulator has also been measured in the VUV spectral range with the ACO storage ring working at its maximum energy (536 MeV). One can see on fig. 9 a typical spectrum showing the harmonics ranking from number 3 to 10. It is appa-

rent that the spectral widths are broadened by the angular dispersion of the elec-
tron beam (it is well-known $\underline{/\ 15\ \underline{/}}$ that the emittance of a storage ring grows with
the energy). It appears also that the harmonics of even rank are as intense as the
odd harmonics although they should vanish in the forward direction in the case of
a linear undulator.

This effect is much stronger at 540 MeV than at lower energies (in the range 150-
240 MeV) where the 2nd harmonic intensity, for example, has been found to be only
10 % to 20 % of the 1st harmonic. This is probably due not only to the increased
emittance of the beam at 540 MeV but also to some detector misalignement and solid
angle acceptance. A more detailed analysis of the VUV emission properties will be
published later on.

On figure 9, the harmonics of rank higher than 7 are very small in comparison
with the theory (see fig. 24 in section V). This is due to the spectral response
of the monochromator which falls off for wavelengths smaller than 200 Å. At 240 MeV
harmonics ranking as high as number 23 have been observed. We conclude this undu-
lator will constitute a suitable source of radiation in the VUV region in the range
1000-80 Å. Absolute measurements of its brillance are now underway.

Gain Measurements

The optical gain experienced by an external argon laser beam aligned collinear with
the electron beam inside the undulator has been measured with the new permanent
magnet undulator NOEL. The experimental method has already been described $\underline{/\ 3,4,5\ \underline{/}}$.
The basic idea behind the gain measurement is recalled here rapidly. A CW argon
laser is made colinear with the electron beam inside the ring (with the aid of
two optical transport lines through the bending magnets). If there is gain (or
absorption) a high frequency modulation appears on the laser light. This frequency
is just the electron bunch revolution frequency in the ring (27.2 MHz). A lock-in
detection is used to measure the signal. In addition the argon beam is chopped at
a low-frequency and a second lock-in detection is made, in order to eliminate the
high frequency contributions not arising from the argon laser amplification process
such as the spontaneous emission and parasitic signals. The system is calibrated
with the synchrotron radiation. The sensitivity in gain is about 10^{-5}.

A typical gain profile versus the gap of the undulator is shown on fig. 10. The
measured curve agrees very well with the theory, as expected from the spontaneous
emission measurements. Even the small oscillations corresponding to the derivative
of the wings of the spontaneous emission curve are visible and the width of the
curve ($\delta K/K = 0.28$) is very close to its theoretical value (0.27). The peak gain $\hat{G}$
is found experimentally to be :

$$\hat{G}_{peak} = 1.5 \times 10^{-4}$$

From the classical theory of the FEL's gain the numerical value of the gain can be
expressed as :

$$\hat{G}_{th} = 0.127 \times 10^{-15} \left(\frac{L}{E}\right)^3 \lambda_o B_o^2 \rho_e F_f \qquad (4)$$

the length L of the undulator, being expressed in meters, E in GeV, the undulator
period λ_o in cm, B_o in Tesla and ρ_e in cm^{-3}. F_f is the filling factor which can be
calculated from the overlap integral between the electron and laser beams. For
coaxial gaussian beams :

$$F_f = \frac{1}{\sqrt{\left[1+\left(\frac{w_o}{2\sigma_h}\right)^2\right]\left[1+\left(\frac{w_o}{2\sigma_v}\right)^2\right]}} \qquad (5)$$

w_o is the laser beam waist and σ_h and σ_v the electron beam transverse sizes.

The measured electronic density, versus different currents in the storage ring, is
shown in fig. 11. The parameters of interest (transverse sizes and length of the

Figure 9 - Spectral distribution of the light emitted in the VUV region by electrons of 536 MeV, for an undulator gap of 325 mm, at $\Theta \simeq 0$. The spectrum has not been corrected for the monochromator spectral response.

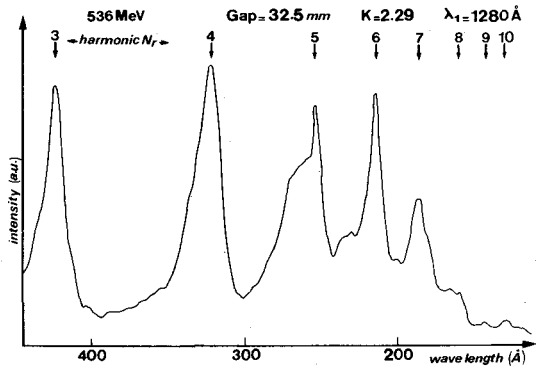Figure 10 - Curve of the gain experienced by an argon laser beam propagating colinearly with the electron beam inside the undulator. The curve is drawn with respect to the undulator gap.
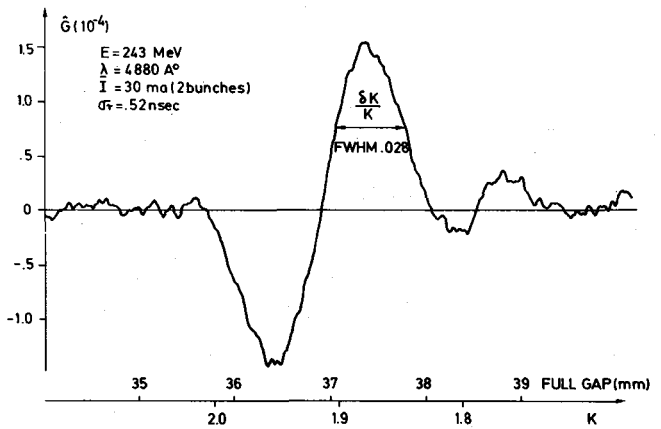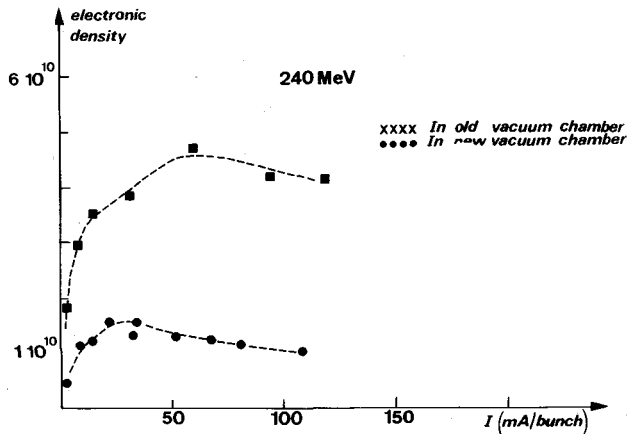
Figure 11 - Measured electronic density in the undulator with a cylindrical vacuum chamber, 200 mm large in diameter, and with a rectangular vacuum chamber, 25 mm high in its smaller dimension, used with the NOEL undulator.

beam) have been measured before the installation of the undulator, with a cylindrical vacuum chamber, and after this installation, with a new vacuum chamber (cf. figure 3). The huge loss in electronic density arises probably from the higher electrical impedance of the new chamber.

From the measurements, with $w_0 \simeq 0.8$ mm, the filling factor for the current at which the electronic density is maximum is :

$$F_f = 0.8$$

and the corresponding value of the gain is :

$$G_{peak} = 2.5 \times 10^{-4} \text{ at } 632 \text{ nm}$$
$$= 1.7 \times 10^{-4} \text{ at } 488 \text{ nm}.$$

This last value is in very good agreement with the measured one, the small discrepancy falling within the uncertainty in the electron beam dimensions for the calculation of the theoretical gain. However this gain value is smaller by a factor of three than was expected from the measurements of the electron density in the ring before installation of the undulator.

We plan to improve the electron density in the near future by "smoothing" the undulator vacuum chamber and possibly by inserting a second, high frequency, RF cavity in the storage ring.

It would be very difficult to make the system oscillate with such a low gain even with a high quality optical cavity (see section VI). For this reason we have tried to enhance the gain by modifying the undulator and operating it as an optical klystron.

III - BUNCH LENGTHENING MEASUREMENTS

Laser induced bunch lengthening is believed to play a critical role in the determination of the power output and efficiency of storage ring FEL's. In a non-isochronous storage ring FEL, the energy spread induced by the laser is believed to set an upper limit to the laser power output and efficiency. Analyses of the mechanism have been published for the idealized SRFEL by Renieri, Elias, and others $/\bar{\ }5,16,17,18,21\_\bar{7}$. In order to test these theories, and to establish an experimental data base for future development of the SRFEL we have devised a sensitive method to measure the laser induced change in the electron bunch length. This method is capable of measuring the absolute bunch with a precision of 1 %, and fractional changes in electron bunch length as small as 1 part in 10^5. While the results that we have obtained agree with the theory in the low current region, the parameters which determine the electron bunch length and energy spread as a function of current can lead to a number of anomalous effects at high current, including laser-induced bunch shortening.

The experimental set up is shown in fig. 12. That part of the experimental set up which concerns the external laser, undulator and the storage ring is similar to the one used for gain measurements on ACO $/\bar{\ }3\_\bar{7}$. An argon ion laser is coupled to the electron beam in the undulator through a mode matching telescope system and optical transport system. Synchrotron light from a bending magnet on the storage ring is detected on a fast photodiode. The detector's location at the bending magnet was chosen to prevent any spurious light from the laser or undulator from reaching the photodiode. The signal from the photodiode is sent via a low dispersion coaxial cable to an AILTECH 757 RF Spectrum Analyzer. The analyser is interfaced directly with the computer used for data aquisition for global spectrum analysis. When monitoring the bunch length changes, the analyzer is operated in the receiver mode tuned to a harmonic of the orbit frequency. The analyzer output can either be fed into a lock-in amplifier for synchronous detection at the frequency of the laser chopper, or be time averaged using an averaging digital oscilloscope. In all cases the detected signal is fed into the data aquisition system together with the storage ring parameters including the RF voltage, the storage ring current, and the output power of the external laser.

The synchrotron light emitted by the electrons in a bending magnet of the storage ring has the form of a series of pulses whose period is fixed by the orbit frequency
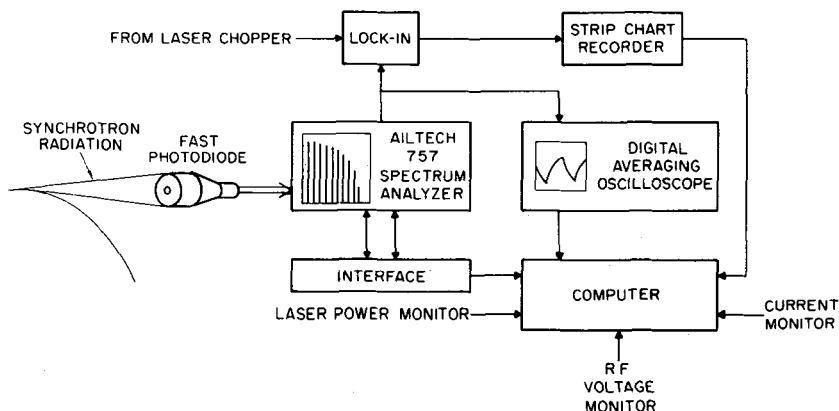
Figure 12 - Schematic of the bunch lengthening experiment

and whose envelope is determined by the electron bunch shape. The Fourier transform of the signal from the photodiode will be a comb spectrum whose envelope (corrected for the photodiode's frequency response) will be the Fourier transform of the electron bunch shape. Fig. 13 shows the global frequency spectrum of the signal from the photodiode. This data is not compensated for the photodiode response.
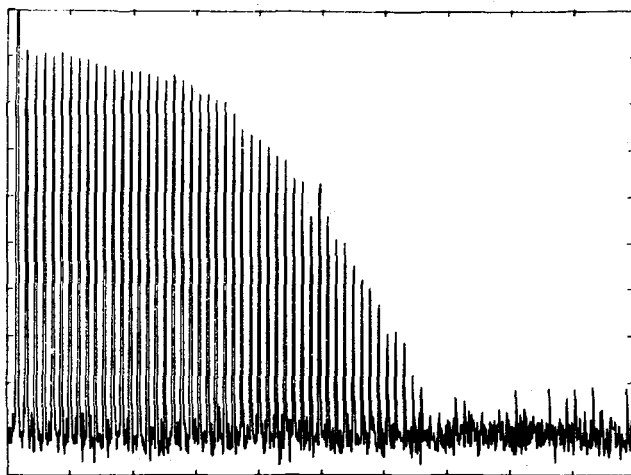
Figure 13 - Spectrum Analyzer output showing the comb spectrum of the photodiode signal from the storage ring synchrotron radiation. The horizontal scale is 100 MHz/div ; the vertical is 5 dB/div. The first line is the zero frequency reference line and subsequent lines are spaced at 13.618 MHz the orbit frequency of the storage ring. The spectral envelope corresponds to a compensated temporal bunch length of 665 picosecond with a mean-square correlation of 99.2 %. The spectrum was taken at an electron energy of 536 MeV, a current of 90 mA, and an RF accelerating voltage of 17.5 kV.

Under idealized condition, the electron pulse shape should be gaussian $\underline{/\ 15\ \underline{/}}$ and
the Fourier transform of the synchrotron light should have a gaussian envelope. The
measurements on ACO confirm this model to high precision. For a typical 200 pico-
second electron bunch, the envelope of the Fourier transform, corrected for photo-
diode frequency response, can be least-squares fit to a gaussian with an uncer-
tainty below 2 % and a mean-squared correlation exceeding 98 %. In fig. 13 the en-
velope shown corresponds to a temporal bunch length of 665 picoseconds. The mean-
squared correlation is better than 99 %.

Assuming a gaussian electron bunch shape, the power spectrum $F(\omega)$ of the photodiode
output will have the form :

$$F(\omega) \propto P(\omega)\ e^{-\omega^2 \sigma^2 / 2}$$

where $P(\omega)$ is the response of the measuring system, σ the temporal bunch length,
and ω the detection frequency. If the detection frequency is fixed and the temporal
bunch length changes from σ_i to σ_f, the detected signal varies with the electron
bunch length as

$$\ln\left(\frac{F_f(\omega)}{F_i(\omega)}\right) = -\frac{\omega^2}{2}\ \Delta\sigma^2$$

where $\Delta\sigma^2$ is defined as $\sigma_f^2 - \sigma_i^2$. The fractional change in signal amplitude is de-
termined by the absolute change in the bunch length, and scales as the square of the
detection frequency. Note also that the fractional change in the detected signal is
unaffected by the response of the photodiode.

Given the value of $\log F(\omega)$ at a particular frequency, bunch length change measu-
rements can be performed in several different ways. Steady-state measurements can
made simply by monitoring the dc component of the signal. This was the method used
in the first measurements made by this system in May 1981, using the superconducting
undulator originally mounted on ACO $\underline{/\ 5\ \underline{/}}$. Synchronous detection can also be used, by
chopping the external laser at a frequency below the energy damping rate of the ring,
and by using a lock-in detector to measure the amplitude of the resulting periodic
change in $\log F(\omega)$. The time response of the electron beam to the chopped laser
beam can be measured by recording the time-dependent waveform of $\log F(\omega)$ on an
averaging oscilloscope.

The sensitivity and precision achievable by these frequency domain measurements is
superior to that achievable with the available temporal methods. While streak came-
ras have comparable resolution, precise absolute measurements require multiple cor-
rections for electron transit time spread and film density. No such corrections are
required in our frequency domain measurements in which transit time spread in the
photodiode has no effect on the detected signal.

Measurements were performed in the low, moderate, and high current regimes. Fig. 14
shows the time averaged response of the electron bunch length to the chopped exter-
nal laser in the low current region (less than 1 mA total average current).

Note that a fall in $F(\omega)$ in Fig. 14 signifies an increase in the bunch length. The
signal shown in fig. 14 indicates a steady state bunch lengthening of 5 %. The
magnitude of the bunch lengthening and the exponential response of the signal appear
consistent with existing bunch lengthening models $\underline{/\ 5,16,17,18\ \underline{/}}$.

Fig. 15 shows the experimental and theoretical bunch lengthening curves at low
current and the spontaneous emission power at the external laser wavelength as func-
tions of the gap between the pole faces of the permanent magnet undulator. For the
permanent magnet ACO undulator, the wiggler parameter K and resonance energy γ_o can
be computed from the gap spacing using the relations :

$$K = 8.5\ \exp\left[-0.0404\ \text{Gap (mm)}\right]$$

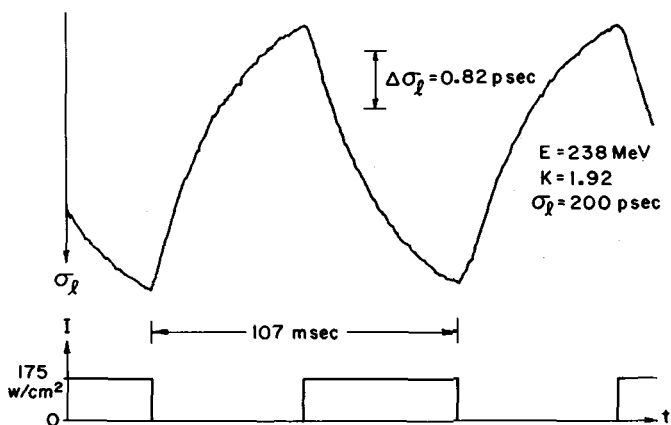$$\gamma_o = \left[\frac{\lambda_o}{2\lambda}\ \left(1 + \frac{K^2}{2}\right)\right]^{1/2}$$

Figure 14 — Time averaged response of the electron bunch length at low current. The upper trace shows the time dependence of log F (ω), the power output of the photodiode detector at the 1062.2MHz harmonic of the orbit frequency. As described in the text, an increase in the bunch length reduces the amplitude of log F (ω). The lower trace records the laser intensity incident on the electron beam.

Theoretically the bunch lengthening curve and the spontaneous emission curve should have the same functional form / 5 /. This prediction is also confirmed by fig. 15. Note that the maximum of the curves occur at a gap of 36.7 mm which corresponds to a K of 1.93. The maximum signal shown corresponds to a bunch lengthening of 6 %. The experimental curve in fig. 15 was recorded using synchronous detection.

In the moderate and high current regimes, important anomalous effects appear which are not accounted for by the simple bunch lengthening theory. These effects include space charge modifications to the RF accelerating potential, and the interactions of the electron beam with the electromagnetic modes of the vacuum cavity. The omission of these effects in the existing bunch lengthening models results in their failure as the current is raised. Fig. 16 shows the response of the electron beam to the external laser at three different operating points in the moderate current regime. Fig. 16 a and 16b may be compared directly to fig. 14 since they have identical chopping periods. The vertical scale of fig. 16a, b and c are 1.57, 0.5, and 2 times that of fig. 14 respectively.

Note that the bunch lengthening signal in fig. 16a is 180° out of phase with the signal in fig. 14. This phase change is reproducible and indicates the electron bunch length was reduced by the external laser. In contrast to the electron bunch heating in fig. 14, the laser cooled the electron beam in fig. 16a.

The response of the electron beam varies as the current decays and various thresholds that are present in the anomalous bunch lengthening regime are crossed / 19 /. Anomalous bunch lengthening effects are seen in ACO when the average stored current exceeds 1 mA. Another typical phenomena in this regime is that shown in fig. 16b. Here a complicated multiple time constant structure appears in response to the laser. Fig. 16 c shows oscillations in the bunch length which also occur in the anomalous regime.

While the low current bunch lengthening data is consistent with existing theoretical models, the qualitative and quantitative discrepancies at high current indicate that effects present in this regime can dramatically alter the excitation of the electrons by the laser. These results indicate that the theoretical models must be

Figure 15 -

a) Bunch lenghtening as a function
of undulator gap. The maximum
signal corresponds to a bunch
lengthening of 6 %, occurring
at a gap of 36.7 mm or equiva-
lently K = 1.93.

b) Spontaneous emission of the per-
manent magnet undulator as a
function of undulator gap at
fixed frequency (5145 Å)

c) Theoretical bunch lengthening
as a function of undulator
gap. The divisions indicated
on all three curves corres-
pond to 1 mm change in undu-
lator pole face gap.

(a) BUNCH LENGTHENING

(b) SPONTANEOUS EMISSION

(c) THEORETICAL
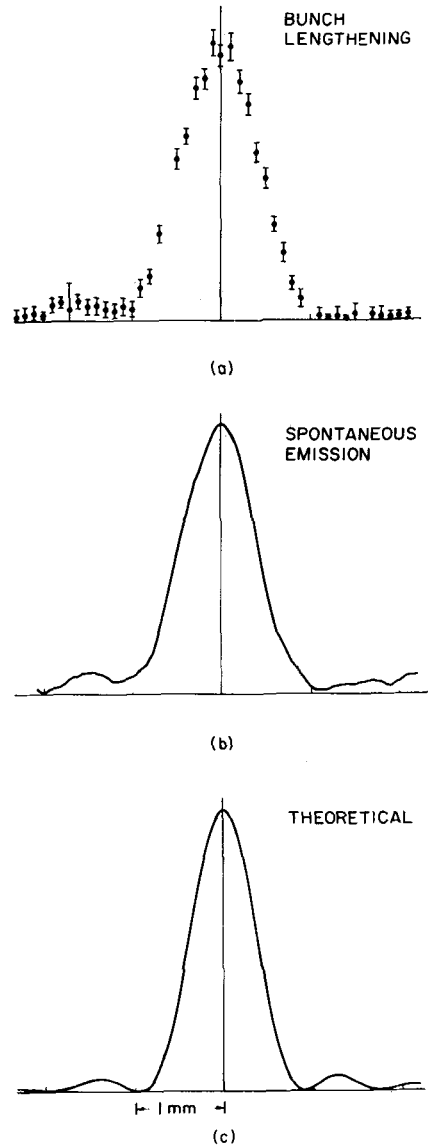
modified to include high current effects. It is possible that the observed laser-
induced cooling may have significant practical implications for storage ring FEL's
and in synchrotron radiation and colliding beams research where it is desirable to
maximize the charge density at high current.

IV - OPTICAL KLYSTRON

An optical klystron has been realized on the Orsay system to increase the gain per
pass which is limited by the short length of the straight sections. This objective
is made possible due to the low natural energy spread of the ACO storage ring. We
report here the optimization of the dispersive section and discuss the spontaneous
emission measurements taken during the last two experimental shifts before the summer

shut-down. An oscillation experiment has also been carried out with the klystron, and the results are reported in section VI.

We use the notation of the theoretical description of optical klystrons in reference /̄ 9,20_/̄

Optimization of the dispersive section

The decision was made to build the dispersive section with the same type of permanent magnets as used for the undulator /̄ 6_/̄ (dimensions 50 x 19 x 19 mm, remanent field ∿ 0.85 Tesla, from BBC-Recoma) for two main reasons :

- a high enough magnetic field turned out to be impossible to achieve with regular electromagnets without an expensive water cooling system.
- the use of the same technology as for the undulator sharply reduces the construction time.

The permanent magnet system has the disadvantage of having a constant field that

Figure 16

Time averaged response of electron bunch length to an externally chopped laser in the anomalous bunch lengthening regime. The upper trace in all three photographs shows the response of log F (ω) (increasing bunch length downward) to the chopped external laser beam recorded in the lower trace of each photograph.

a) 2.5 mA average current, RF voltage of 4.0 kV, and chopping period of 107 msec.

b) 2 mA, 5.76 kV, and a chopping period of 107 msec

c) 2.5 mA average current, 12.0 kV RF, and a chopping period of 560 msec (only the laser "on" portion is shown)

5 mV/div (a)

5 mV/div (b)

20 mV/div (c)
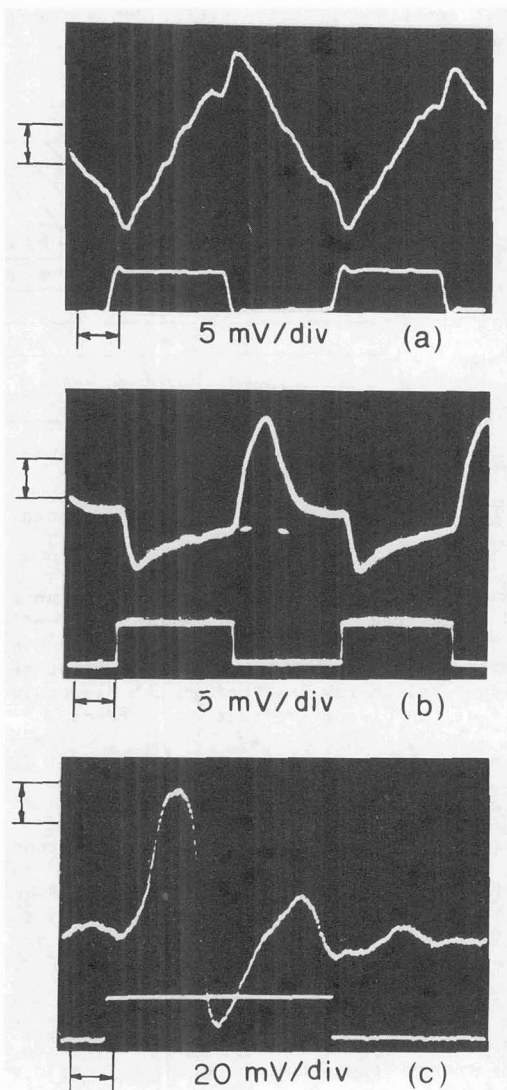
can only be changed by adjusting the gap between the jaws. The use of the same mechanical system for undulator and dispersive section couples the undulator and dispersive section field variations with the gap and only permits a one-time adjustment of the relative field amplitudes.

As in the case of the undulator, the magnets were first paired and glued into 100 x 19 x 19 mm magnet bars, and then arranged as described below to form the dispersive section. The three central periods of the original 17 period undulator had been made physically separable from the others / 6 /, for this purpose and could be easily removed to make way for the 12 magnet long dispersive section.

We have studied the configuration of{ $\frac{n}{2}$, 6-n, n, 6-n, $\frac{n}{2}$ } magnet elements arranged vertically and horizontally as {+ V, + H, − V, − H, + V } respectively (see fig. 17 which presents two layers of such a configuration for n = 3). This configuration was chosen because if n is an integer, the smallest magnet element is a half pole, the above distribution gives twelve elements, and is automatically compensated for orbit angle and position deviations since the field integral is zero and the field is symmetric with respect to the middle.
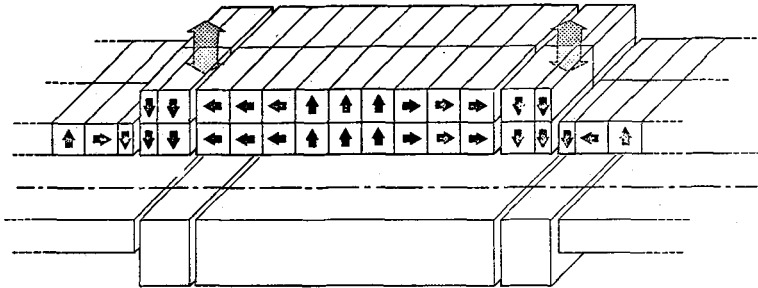
Figure 17 - Dispersive section permanent magnet configuration optimizing
             the gain

The magnetic field was calculated using an electrostatic-like potential calculation code described in ref. / 6 /. For each configuration we calculated N_d the dimensionless parameter that determines spontaneous emission spectrum and gain / 20 /. N_d represents the number of periods of light of wavelength λ passing over an electron which total energy is γmc^2 in the dispersive section. For light propagating on the axis of the dispersive section it reads :

$$N_d = \frac{1}{2\lambda\gamma^2} \left(d + \frac{e^2}{m^2 c^2} \int_{-\infty}^{+\infty} \left[\int_{0}^{u} B(z) \ dz \right]^2 \ du \right) \qquad (6)$$

where m is the electron mass, e the electron charge, c the speed of light, d is the dispersive section length (12 magnets long) and B(z) the vertical magnetic field created by the dispersive section magnets at the longitudinal coordinate z. B(z) and therefore N_d are calculated on and off axis of the dispersive section. The table 2 gives the calculated on axis N_d at λ = 6328 Å, γmc^2 = 240 MeV for one layer of magnets with a remanent field of 8.5 kG and a gap of 32 mm.

The optimal value of n = 3 was chosen for our system. The table 3 shows N_d for n = 3 and m layers of magnets. We have also calculated σ_γ/γ the corresponding relative energy spread for which the O.K. gain would be optimized, using the formula (6)

$$N_d = \frac{1}{4\pi \frac{\sigma_\gamma}{\gamma}} - N$$

where N = 7 is the number of periods of one of the two identical undulators constituting the optical klystron.

Table 2

n	0	1	2	3	4	5	6
Nd	20.1	25.3	29.9	32.7	31.2	26.0	18.4

Table 3

m	N_d	$\frac{\sigma_\gamma}{\gamma}$
1	32.7	2×10^{-3}
2	79	9.3×10^{-4}
3	114	6.6×10^{-4}

Since the ACO energy spread is close to 10^{-3} at nominal current, we chose m = 2. Fig. 17 shows the retained configuration.

Each magnet of the external layer (the one farthest from electron beam) was individually glued on an aluminium piece that was clamped on a bench as for the undulators. Magnets of the internal layers were glued to those of external layers. Because of the remanent field variation in magnitude and direction, the magnets were individually measured and a careful pairing was done to compensate for the horizontal components of the field /‾6‾/. The two jaws were made as symmetric as possible and the strongest magnets were placed on the ends to allow final orbit compensation by moving these adjustable magnets away from the axis of the electron beam (see fig. 17).

The measured magnetic field was very close to the calculated field (shown on fig. 18) for the whole optical klystron) with a 1.08 field scaling factor that could originate from a misestimate of the magnets' remanent field for the calculation. The calculated trajectory is shown in fig. 18, which shows a large wiggle of about 2 mm amplitude for an electron energy of 240 MeV and a gap of 33 mm.

Spontaneous emission measurement

Figure 19 shows a spontaneous emission spectrum at an energy of 240 MeV for a gap of 37.79 mm at low current in the ring.

We have compared the envelope of the oscillations with that of the emission spectrum of a perfect undulator having exactly N sinusoidal periods, the field outside these periods being exactly zero. The emission spectrum $dI/d\lambda$ of such an undulator is :

$$\frac{dI}{d\lambda} \propto \frac{1}{\lambda^4} \left(\frac{\sin \delta}{\delta}\right)^2 \qquad (7)$$

with $\qquad \delta = \pi N \left(1 - \frac{\lambda_R}{\lambda}\right)$

where λ_R is the resonant wavelength. Fitting the envelope to curves given by (7) gives N = 8.1 ± .1 instead of 7. This discrepancy is probably due to the dispersive section field which could be partly resonant with the other 7 periods. It is certain-
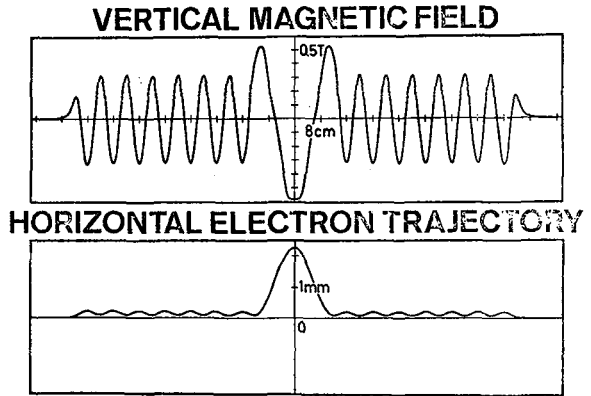
VERTICAL MAGNETIC FIELD

Figure 18

Vertical magnetic field
calculated *for the Orsay optical*
klystron (gap = 33.00 mm) and
the corresponding calculated
horizontal electron trajectory
at an energy of 240 MeV.

HORIZONTAL ELECTRON TRAJECTORY

Figure 19

Spontaneous emission $\dfrac{dI}{d\lambda d\Omega}$

of the Orsay optical klystron
measured for an electron
energy of 240 MeV and a magnetic
gap of 37.79 mm. The current
decay I(t) is superimposed.
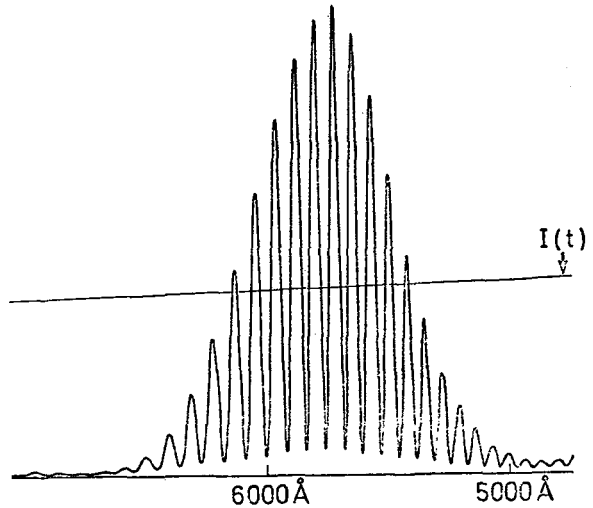
ly not due to the fringe field of the half periods which slightly decreases the ef-
fective number of periods. The envelope of oscillations also presents a long lower
wavelength tail with the secondary maximum amplitude lower than expected. This effect
was also seen in the 17 period undulator emission curves and might be due to the
field imperfections or residual transverse field components. Similar curves of emis-
sion were obtained as function of energy or field in the dispersive section (by
changing the gap).

Plotting the number of the maxima as a function of $\frac{1}{\lambda}$, we verified a high linearity
of N_d as a function of $\frac{1}{\lambda}$ (0.9999 correlation coefficient in the range $0.3 < \lambda < 0.7\,\mu$).
From the slope, we can calculate the experimental values of N_d which is
$N_d = 65.3 \pm 0.2$ at $\gamma mc^2 = 240$ MeV and $\lambda = 6328$ Å for a dispersive section gap
of 35.00 mm. This value is close to the value $N_d = 68$ predicted from the field mea-
surements. The discrepancy could be due to the Hall probe calibration, the storage
ring energy calibration, or the error in the calculation of N_d produced by neglec-
ting the undulator field in the fringe field of the dispersive section. Note that
these values are lower than in table 3 because the gap is wider. The resonance bet-
ween the electrons and the light at $\lambda = 6328$ Å can be maintained at low energy by

increasing the gap (to decrease the undulator field). From field calculations one expects $N_d \simeq 86$ at 150 MeV, and in fact we measured $N_d \simeq 84 \overset{+}{-} 5$.

No beam time has yet been available to make direct measurements of the gain of the klystron. However, evidence of improvement of the optical klystron gain compared to the undulator gain has appeared in the spontaneous emission amplification experiments (section VI). From the spontaneous emission curves, one can expect a maximum gain enhancement of 5.2 f compared with the 17 periods undulator at 240 MeV and $\lambda = 6328$ Å, the factor f < 1 represents the gain decrease due to inhomogeneous broadening $/\ 9,20\ /$. This factor can be accurately deduced from the emission spectrum which is proportionnal $/\ 20\ /$ to 1 + f cos $(2\pi N_d)$.

Assuming the contributions to inhomogeneous broadening to be independent and weak, f reads $/\ 9\ /$

$$f = f_m \times f_B \times \exp \left(- \frac{\sum_i \sigma_i^2}{2} \right) \qquad (8)$$

where the index i distinguishes the different sources of inhomogeneous broadening. f_m is the modulation decrease due to the monochromator. f_B is the one due to O.K. and dispersive section field imperfections emission.

For an on axis beam and zero observation angle, one has $[\ 9,\ 20\ ]$

$$\sigma_1 = 4\pi (N + N_d) \frac{\sigma_\gamma}{\gamma} \qquad \text{(energy spread contribution)} \qquad (9)$$

$$\sigma_2 = \pi \frac{(L + d)}{\lambda} \sqrt{2} \ \sigma_{\theta x}^2 \qquad \text{(horizontal angular spread contribution)} \quad (10)$$

$$\sigma_3 = \pi \frac{(L + d)}{\lambda} \sqrt{2} \ \sigma_{\theta y}^2 \qquad \text{(vertical angular spread contribution)} \quad (11)$$

$$\sigma_4 = 4\pi(N + N_d) \sqrt{2} \ q_x \ \sigma_x^2 \qquad \text{(horizontal beam dimension contribution)}$$

$$(12)$$

$$\sigma_5 = 4\pi(N + N_d) \sqrt{2} \ q_y \ \sigma_y^2 \qquad \text{(vertical beam dimension contribution)}$$

$$f_m = \frac{\sin^2\alpha}{\alpha^2} \times \exp \left[- \left(\frac{\pi}{12} \frac{L + d}{\lambda} a^2 \right)^2 \right] \qquad \begin{array}{l}\text{(monochromator band pass and angular} \\ \text{aperture contributions)} \qquad (13)\end{array}$$

with

$$\alpha = \pi(N + N_d) \frac{\Delta\lambda}{\lambda}$$

where L is the undulator length, d the dispersive section length, $\sigma_{\theta x}$ and $\sigma_{\theta y}$ the horizontal and vertical RMS angular spread of the electron beam, σ_x and σ_y the horizontal and vertical RMS beam transverse dimensions, q_x and q_y are field dependent factors noted Q_x and Q_y in ref $/\ 9,\ 20\ /$, $\Delta\lambda$ is the monochromator FWHM and a its total angular aperture ($\sim$ the diameter of a pinhole divided by the distance to the O.K.).

We assume the horizontal and vertical axis are the proper axis of the ellipse representing the electron beam in the transverse plane. In the rare cases where it is not true, one would have to take x and y for the real proper axis.

$q_y \simeq 3.4 \times 10^{-4}$ mm^{-2} was deduced from field measurement, this value is just 10 % lower than that anticipated from the field calculation. These calculations also predicted $q_x \simeq 8.4 \times 10^{-5}$ mm^{-2}, a value that has been roughly confirmed by the field measurements. Taking $\sigma_x = \sigma_y = 0.35$ mm, one has :

$$\sigma_4 = 0.012$$

$$\sigma_5 = 0.053$$

Therefore, using an appropriate monochromator bandwith ($\Delta\lambda \sim 4$ Å in our case), the most important contributions come from the energy and the angular spread :

$$\sigma_1 = 890 \times \frac{\sigma_\gamma}{\gamma}$$

$\sigma_2 = 0.23$ }   For typical low current theoretical horizontal and vertical
$\sigma_3 = 0.06$ }   beam divergences of 0.2 and 0.1 mrad.

On ACO at 240 MeV, the energy spread increases from 2×10^{-4} ($\sigma_1 = 0.18$) at very low electron current to more than 10^{-3} ($\sigma_1 = 0.89$) at high current. The decrease of the modulation rate of the spontaneous emission curve as a function of current has been experimentally confirmed, giving $\sigma \simeq 0.78$. This value, taken at 240 MeV with an average current of 100 mA in two bunches with sextupoles, corresponds to a relative energy spread of 8.6×10^{-4}.

The angular divergence contribution was also checked by artificially increasing the beam divergence. This can be done either by exciting transverse oscillations in the beam by using a broad band noise source applied to an electrode in the vacuum chamber, or by acting on the quadrupole current to change the beam focussing.

An estimation of f_0 can be obtained by operating at extremely low current and taking all precautions to minimize the inhomogeneous effects. The best modulation rate obtained is $f \simeq 0.935$. If we substract the theoretically calculated effects due to energy spread, angular spread and monochromator bandwidth, we find $f_m \lesssim 0.98$. This confirms that the dispersive section was well compensated.

In the usual case $N_d \gg N$, one finds from equations (9) to (13) that σ is always proportional to $1/\lambda$ except for the monochromator contribution proportional to $1/\lambda^2$. This proportionality was verified by calculating σ from the measured modulation rate on the first three harmonics. After deconvolution with the monochromator response we obtain in the same experimental configuration :

Harmonic number	Fundamental	2nd	3rd
σ	0.73	1.45	2.09

This table confirms the optimisation of the dispersive section strength on the fundamental. The modulation rate and therefore the bunching efficiency decrease in the U.V. An optimization of the gain on the 3rd harmonic would necessitate a lower dispersive section field.

For an off-axis injected beam σ_2, σ_3, σ_4 and σ_5 are larger [9,20]. The useful aperture of the optical klystron has been found experimentally by observing the dependance of the modulation on the observation angle. Defining the aperture as the domain in which $\sigma < 1$, which means the gain and modulation rate are decreased by less than $e^{-.5} \simeq 0.6$, we find :

horizontal aperture = $\pm$ 20 mm

vertical aperture   = $\pm$ 4.7 mm

angular aperture   = $\pm$ 0.6 mrad

V -- MEASUREMENTS OF THE FEL CAVITY Q DEGRADATION

From the start of the Orsay FEL project, it has been clear that extraordinary measures would be needed in order to succeed in an audacious enterprise to achieve laser oscillation in the first machine of its kind - a storage ring laser - on a

system on which the maximum round-trip gain available was on the order of 10^{-4}. The implications were clear : all possible loss mechanisms in the optical cavity had to be reduced to a minimum and the highest possible gain had to be achieved. Furthermore, it was apparent that precise measurement systems had to be designed and implemented to permit measurements of both the gain and the cavity losses. The gain measurements was needed to verify the numerical factors in the theory and the optical cavity measurement was required to show whether the high Q of a mirror pair could be maintained despite exposure to the radiation environment produced by the operation of the storage ring and the undulator.

As a response to these needs, the optical cavity was constructed of two mirrors inside the 10^{-10} torr vacuum of the storage ring ACO in order to eliminate the losses inherent in a set of intracavity Brewster windows. The gain, which is small due to the short length of the straight sections in ACO, has been optimized through the implementation of a set of beam-stabilizing sextupoles in the storage ring magnetic lattice ; the measurement and selection of the optimum operating point as a function of machine energy and current;and the installation of an optical klystron as was discussed in the third section of this review.The gain measurement system and some of the results have already been reported $/$ 3,4,10 $/$ and are by now well known. It is the purpose of this section of our review to discuss the cavity measurement systems we have constructed and to present the first results.

Q measurement techniques

We have worked with four mirror pairs, as shown in table 4, during our experiments with the high-Q optical cavity. These mirrors were polished to have the lowest possible surface roughness, and were coated with (typically) 24 layers of TiO_2 and SiO_2 to produce high reflectors optimized at either 6328 Å or 5145 Å. These wavelengths were chosen to permit measurements of the cavity Q with an external laser. The radius of curvature is either 3 or 6 m and the usable diameter of the coated surface is 16.5 mm.

We have used two independent techniques to measure the quality factor or Q of the optical cavity. The first technique uses the spontaneous emission of the undulator which is adjusted to emit at the center wavelength of the mirrors. The axis of the optical cavity is aligned to the axis of the electron beam propagating in the undulator, and the spontaneous emission fills a certain number of eigenmodes of the cavity. The intensity in each of these modes builds up until the losses per round trip equal the spontaneous intensity radiated into that mode per round trip. Despite the fact that the transmission of the mirrors is typically 3×10^{-5} the cavity Q is large enough to create an intense stored beam whose transmitted intensity is clearly visible to the naked eye. It is through the intensity and symmetry of this spot that the cavity is aligned on the electron beam.

Table 4

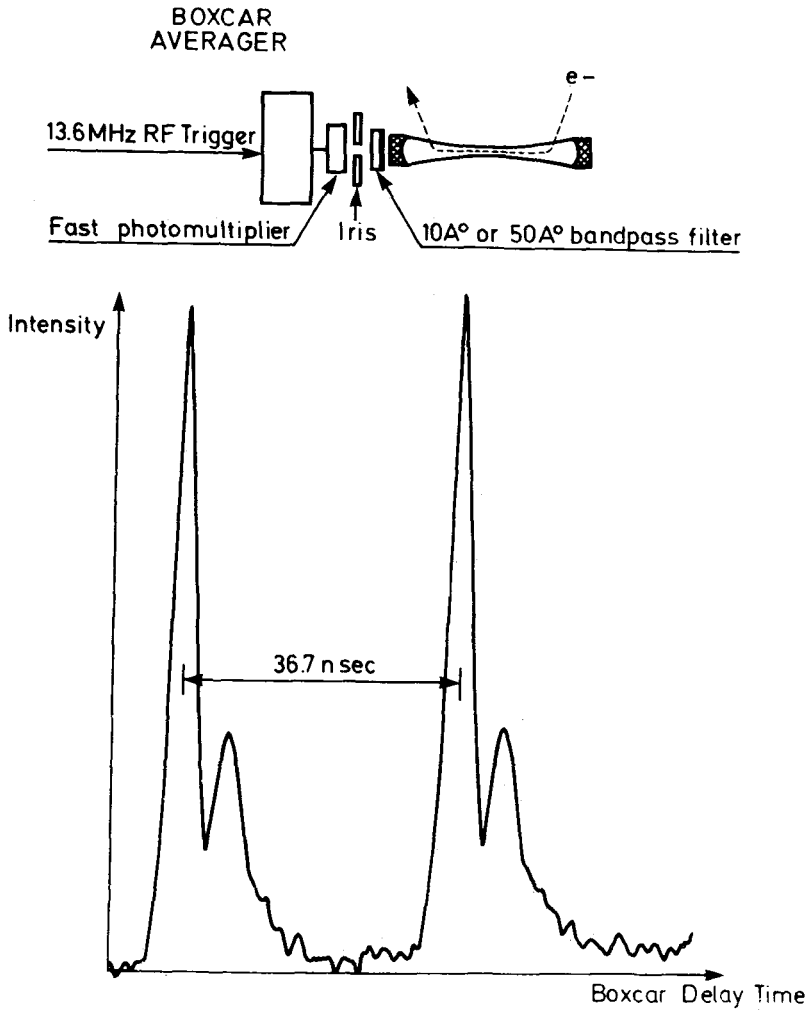| Mirror pair	A1δ , A2δ	A4δ , A5δ	Z6α , Z7α	B1ε , B2ε
Dates of insertion and extraction from storage ring vacuum	1 Apr–26 May	26 May-7 June	7 June-23 July	23 July-present
Wavelength of transmission minimum	6250 Å	6250 Å	5090 Å	6330 Å
Substrate surface roughness (RMS)	∿ 2 Å	∿ 2 Å	4 Å	∿ 2 Å
Radius of curvature	6.8m	6.8m	5.34m	3.0m
Substrate material	Zerodur		Borosilicate Glass B16-64	Suprasil II

Figure 20 - At the top is a schematic of the apparatus used to measure the cavity
           Q of the FEL optical cavity. The curve at the bottom is the time depen-
           dence of the light stored in the cavity once the mirror separation is
           correctly set. The secondary peaks are due to reflections in the elec-
           tronics.

The electron bunch length $\sigma_1 \approx 400$ psec is short compared to the cavity round trip time $T_0 = 36.7$ nsec, so that the cavity Q can be measured by observing the time structure of the stored light. As shown at the top of fig. 20, the light transmitted through a cavity mirror is detected by a fast photomultiplier after filtering out the portions of the spectrum which are transmitted through the cavity mirror with little or no reflection. The length of the ACO storage ring laser cavity can be adjusted to equal precisely one quarter of the storage ring circumference. In this configuration the light pulse emitted on one pass by the electron bunch is superimposed exactly on the pulses stored in the cavity by previous passes, and the stored optical pulse length has its minimum length. By minimizing the observed pulse length at the output of the optical cavity we can adjust the mirror separation to bring the stored optical pulses into superposition with the electron bunch (this technique also solves the length alignment problem for the oscillation experiment - see the next section). A scan taken with a boxcar averager of the time structure of the stored light is shown at the bottom of fig. 20 under the minimum pulse length conditions. The secondary peaks are reflections in the electronics. Note that this experiment is typically performed with two bunches in the storage ring so that a new light pulse is added for each round trip in the optical cavity.

The output mirror of the cavity, which is mounted on a micrometer driven precision translation stage, can be displaced to change the cavity length by a known amount Δl. Now the stored light pulses are longitudinally displaced by $2 \Delta l$ per round trip from the new pulse contributed by the electron bunch on each pass, and as they decay, they create an exponential tail whose decay time τ is related to the cavity Q or the loss coefficient Γ and the mirror displacement by the relation

$$Q = \frac{1}{\Gamma} = \frac{c\,\tau}{2\Delta l} \qquad (14)$$

Two measurements by this method of the total cavity losses Γ are shown in fig. 21.

This technique has the advantage that it can be performed rapidly during the oscillation experiments without disturbing the conditions of optimum alignment. The curves of figure 21 are the convolution of the aligned cavity time structure of figure 20 with a one sided exponential. The data reduction may be simplified by taking advantage of a remarkable property of the exponential : if we convolute the instrument function $f(t)$ which is zero for $t < - \delta$ where δ is related to the width of $f(t)$

$$f(t) = f(t)\; \Theta\; (t + \delta)$$

with a one-sided exponential $g(t)$

$$g(t) = e^{\alpha t}\; \Theta(-t)$$

it follows that :

$$h(t) = f(t) * g(t) = e^{\alpha t} \text{ x constant} \qquad t < - \delta \qquad (15)$$

In other words, the exponential decay visible in figure 21 is, within suitable limits, exactly the decay time of the cavity. A simple fit to an exponential is therefore sufficient to calculate the cavity Q through (14). In practice, precise measurements have been difficult due to the noise present at low signal levels and due to an instrumental baseline drift problem. For this reason, we have also acquired data with another technique which we had developed to measure the mirrors before insertion into the storage ring vacuum.

The second cavity Q measurement method $/\overline{} 22,23 \underline{}/$ is a phase shift measurement on an intensity modulated external laser. The cavity mirrors are aligned onto the laser as a Fabry-Perot, the laser input is modulated at frequency ω with a Pockels cell, and the phase of the intensity modulation of the transmitted beam is measured with the digitized output of a two phase lock-in amplifier. The phase is retarded due to the multiple reflections in the cavity, and the phase shift is related to the total losses in the cavity through the relation

$$\Gamma = \frac{2L}{c} \left(\frac{1}{\tau} - \frac{1}{\tau a} \right) \qquad (16)$$
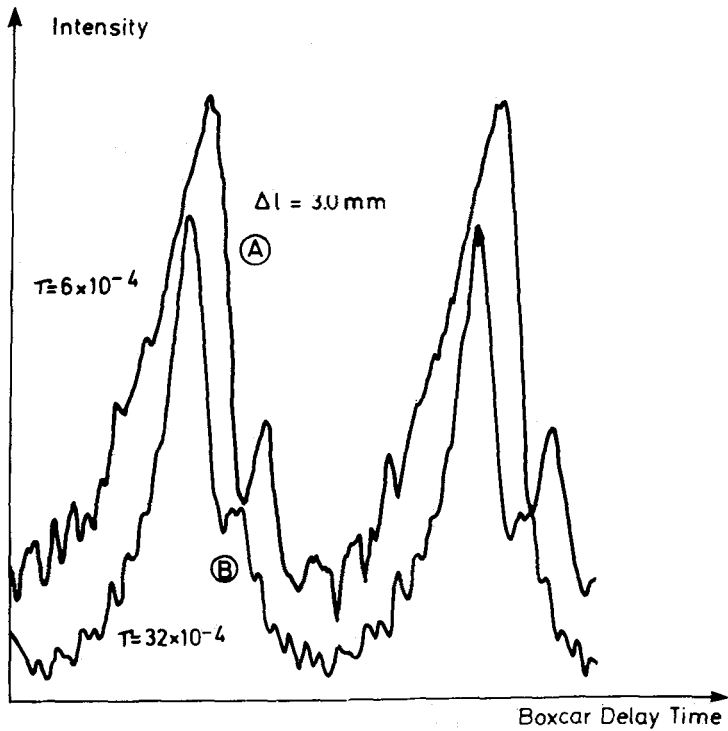
Figure 21 - Two traces of the time dependence of the light stored in the cavity are shown for a cavity length misalignment of 3 mm (the cavity is too short). These curves were taken on the same set of mirrors A) after exposure to the undulator light at K= 0.89, and B) after exposure at K = 2.13 (see table 6). The exponential tail is clearly visible on the left hand edge of the pulses, and the decay time becomes smaller as the losses increase.

where τ , the decay time of the cavity (of length L) is determined from

$$\tau = \frac{\tan\ (\Delta\phi)}{\omega} \tag{17}$$

The absorption coefficient in air, τ_a, must be taken into account for high Q or long cavities.

The method has been tested by measuring the phase shift as a function of the separation of the two mirrors and also as a function of modulation frequency. Fig. 22

shows a plot of $1/\tau$ vs $1/L$ for the best set of mirrors we have obtained $\underline{/}^-24\underline{\,}^-\underline{/}$.

Figure 22 – The inverse cavity decay time is plotted against the inverse mirror se-
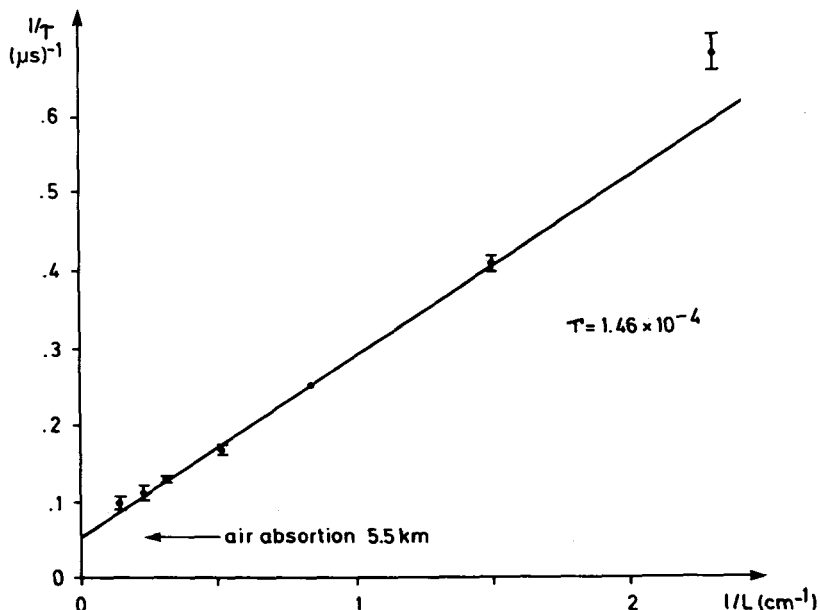paration during one of the measurements of the mirrors B1ε and B2ε , in air. The
curve should be linear, with slope related to the cavity losses Γ and intercept given
by the losses in air .

As expected, the points fall on a straight line, the slope of which gives the losses
of the mirror pair. The result for the total losses is an amazing 7.8×10^{-5} on
average per mirror (transmission + absorption + scatter loss). Other mirror sets we
have measured have been less good (see table 5). The intercept is the absorbtion in
air on the day of the measurement, and is in agreement with the absorption coeffi-
cients given in the Handbook of optics $\underline{/}^-25\underline{\,}^-\underline{/}$. The method has also been verified by
directly measuring the decay time of the light intensity built up in the cavity
which is filled by a laser beam chopped by a pockels-cell. Although the latter method
makes inefficient use of time during the averaging process and is therefore less
accurate, the two measurements agree within the error bars.

The phase shift method is both rapid and precise : in 30 seconds of averaging, we
obtain a measurement with a precision of 1 %. It has been used to measure all
of our mirrors before insertion into the vacuum, and once to measure the performance
of the mirrors in the vacuum. In this latter measurement an argon laser was trans-
versely modematched into the FEL cavity mounted on the storage ring. The experiments
were performed with no electron beam in the ring in order to eliminate the synchro-
tron light which is more intense than the mean transmitted laser power. We expect
that in a future experiment we will be able to perform these measurements in the
presence of the electron beam by filtering out the unwanted synchrotron light and
shifting the undulator radiation wavelength away from the argon line.

Measurement of initial Q degradation

We observe two different problems with the FEL cavity. The first is that the losses increase when the mirrors are placed in the vacuum. Table 5 shows the measurements made on two mirror sets before and after their insertion into the storage ring vacuum. The losses increase by 3 to 7 x 10^{-4} per mirror.

A series of measurements show that exposure to the vacuum itself does not further increase the mirror losses after the initial degradation takes place. The losses were measured continuously for 20 hours after the pumpdown and the opening of the valves which isolate the mirror chambers from the storage ring vacuum.

<div align="center">

Table 5

Average Losses Per Mirror

</div>

	In air	After 10^{-10} Torr Pump Down
Mirrors A4 δ , A5 δ λ = 6250 Å	1.3 x 10^{-4}	8.5 x 10^{-4}
Mirrors Z6 α , Z7 α λ = 5090 Å	4.5 x 10^{-4}	9.9 x 10^{-4}
Mirrors B1 ε , B2 ε λ = 6330 Å	0.8 x 10^{-4}	3.5 x 10^{-4}

No change was observed within the accuracy of 2 x 10^{-5} (A small change was observed due to drift in the laser alignment, but the effect disappeared upon realignment). There is no long term physical degradation in the vacuum such as might be caused by sputtering of Ti from the ion pump. A test was also made for the effect of degassing the hot cathode ionization gauge, with a null result.

At present, the cause of this initial degradation has not been identified. A simple calculation shows that the change in reflectivity is about 50 times larger than could be explained by the bulk index contribution of a 3 % concentration of water vapor trapped in and then pumped out of the coating materials. It remains possible that physical defects such as voids or delaminations are created in the multilayer structure during pump-down, and that these defects increase the scatter losses of the mirror. These possibilities are presently under investigation. It would also appear from table 5 that the mirrors may have been polluted with forepump oil during pump-down, which would add to their absorption. As we improved our techniques, we observed that the initial degradation became smaller, and now all possible measures are taken to avoid backstreaming of pump oil. The mirrors are installed in the chambers under a positive pressure of evaporating liquid nitrogen ; prepumping is accomplished with oil free membrane and sorption pumps followed by a turbomolecular pump ; and the ion pump is started at a pressure of about 1 x 10^{-7} Torr. Titanium sputtering from the ion pump is unlikely during turn-on since no plasma discharge occurs at this pressure. We note in passing that the mirror in the line-of-sight of the electrons receives a typical dose of 75 Roentgens of hard gamma radiation during a short injection of the machine. Again within the precision of 1 x 10^{-5}, no change was observed in the cavity losses before and after such an injection.

Measurement of UV - induced Q degradation

The second major problem observed with the FEL cavity is that its losses increase when the undulator light strikes the mirrors surfaces. Since there is no shift in the transmission curve of the mirrors before and after exposure, either in wavelength or in magnitude, we conclude that the mirror degradation occurs in either the absorption or the scattering channels.

We have made several measurements of the degradation rate, which are summarized in table 6.

In all cases, the mirrors used are multilayer dielectric stacks of $\lambda/4$ optical thickness of TiO_2 and SiO_2 with a $\lambda/2$ overcoat of SiO_2. The mirrors which have been measured vary in peak wavelength and radius of curvature as indicated in table 1. Measured transmission is typically 3.10^{-5}.

The first two columns of table 6 show the degradation rates observed on the same pair of mirrors and under optimal conditions for the measurement. The axis of the laser cavity had been well aligned to the electron beam, and no other measurements distracted our attention so that the experimental conditions were fully documented. This run was planned after the degradation has proceeded to the point where further subthreshold cavity experiments were of no value, and as a result the cavity losses during the experiment, $\Gamma = 4 \times 10^{-3}$, were rather high. The low errors on the measurement of the degradation rate were made possible by using the phase shift method with which we were able to measure small changes in the total cavity losses with an accuracy of 0.5 %. The degradation rate quoted is for the cavity as a whole ; individual rates of change cannot be directly inferred from the data in the first column because the two mirrors receive an unequal dose of high frequency light.

Table 6

Degradation rate of round trip cavity losses (per 100 ma.hr)	6.4×10^{-4} $\pm$ 7 %	1.5×10^{-4} $\pm$ 14 %	$0^{+}_{-}2 \times 10^{-4}$	40×10^{-4} $\pm$ 30 %
Electron energy	238 MeV	238 MeV	150 MeV	230 MeV
Undulator magnetic field parameter	$K = 1.89$	$K = 1.89$	$K = 0.89$	$K = 2.13$
Conditions	FEL operating conditions	Rear Mirror blocked	2 % TiO_2 contamination in SiO_2 layer and vice-versa (data taken with optical Klystron)	
Total exposure	69 ma.hr	115 ma.hr	60 ma.hr	60 ma.hr
Cavity losses before exposure	36.4×10^{-4}	41.2×10^{-4}	7×10^{-4}	7×10^{-4}
Undulator flux at fundamental (1.9eV) (photons/sec/cm^2/ma)	6.8×10^{14}	6.8×10^{14}	3.1×10^{14}	5.6×10^{14}
Flux at 3rd harmonic (5.7 eV)	3.2×10^{14}	3.2×10^{14}	3.7×10^{13}	2.9×10^{14}
Flux at 5th harmonic (9.5 eV)	1.7×10^{14}	1.7×10^{14}	5.0×10^{12}	1.8×10^{14}
Flux at 19th harmonic (36 eV)	4.7×10^{12}	4.7×10^{12}	$\sim 10^{7}$	1.1×10^{13}
Mirror batch	$Z\alpha$	$Z\alpha$	$B\epsilon$	$B\epsilon$

The degradation rate in the second column was measured with an obstruction in place between the two cavity mirrors. Under these conditions, the rear mirror is totally shielded. The degradation rate drops by more than a factor of four. Two explanations are possible for this effect. Either the damaging radiation is stored in the cavity, or the degradation rate slows markedly in the region $\Gamma \simeq 4 \times 10^{-3}$. We do not yet have enough data to distinguish between these two possibilities, and the possibility that the reflection coefficient is large somewhere in the UV cannot be rejected.

Indeed, in the wavelength range above 500 Å (25 eV), SiO_2 by itself has a reflec-
tion coefficient which varies between 5 % and 22 % /‾26‾/, with a sharp peak at
1200 Å. In a multilayer stack it is likely that the phase conditions for high
reflection will be satisfied at one or several harmonics of the undulator. We plan
to measure the reflectance of these mirrors deep into the UV in order to quantify
this hypothesis.

Another prove of the nature of the effect is provided by the results of an experiment
in which a 6328 Å mirror(Alδ) which had previously been exposed, was heated in
air to 285° for 12 hours. The measured losses of this mirror recovered from 12×10^{-4}
to 3.7×10^{-4} after treatment. The remaining losses are close to the value before
exposure to the undulator light but after insertion in the vacuum. These results
prove that the radiation-induced losses seems reversible, but indicate that the ini-
tial vacuum-insertion losses are probably irreversible.

We have verified that the "rear" mirror of the cavity (the one which is not in
the line-of-sight of the electron beam) also degrades with time. The mirror pair
from the batch $Z\alpha$ were measured in air before insertion into the vacuum and again
in air immediately after they were extracted from the vacuum at the end of the
series of experiments with that mirror set. Fig. 23 shows the losses per mirror
which were deduced with the aid of a third known mirror in the phase shift expe-
riment we have described above. The losses were measured as a function of position
on the mirrors by displacing the measured mirror on a grid and realigning the cavity
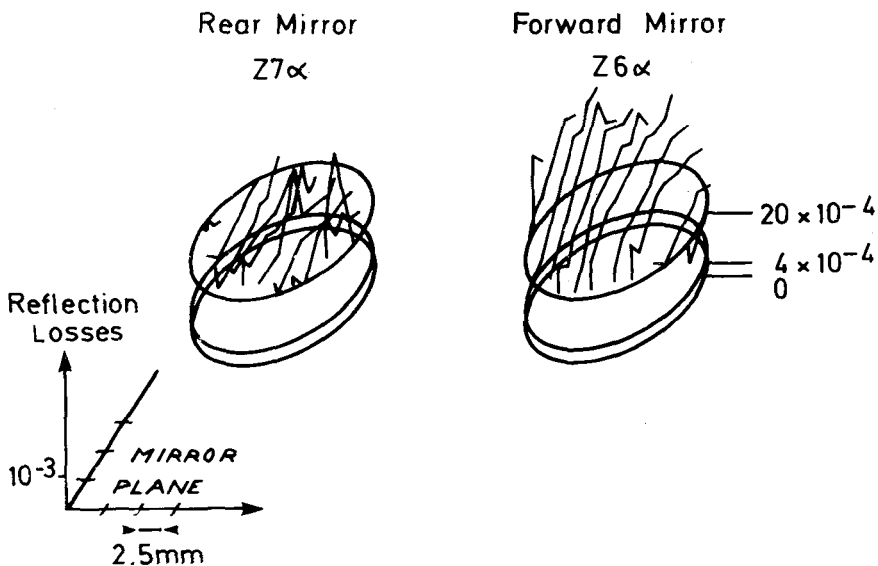point by point.

Rear Mirror

Z7α

Forward Mirror

Z6α

20×10^{-4}

4×10^{-4}

0

Reflection
Losses

10^{-3}

MIRROR
PLANE

2.5mm

Figure 23 – The losses per reflection after exposure of the forward (in the line-
of- sight of the electrons) and rear mirrors are plotted as a function of position
on the mirror surface. The circles represent surfaces of constant reflection loss.
The lower circle, at 4×10^{-4} (R = 99.96 %) shows the loss level per mirror before
exposure, which varies between 6×10^{-4} and 4×10^{-4} across the surface. Degrada-
tion occurs in both mirrors, although it is most severe in the mirror directly
bathed in the undulator light. The data strongly suggests in the losses of the for-
ward mirror the presence of a large hump cut off at the edge by the mirror holder
during the measurement.

There is an extremely sharp increase in the measured losses when the stored mode hits the edge of the mirror holder and diffraction losses become large. The results are presented over the range for which the diffraction losses in the measurement system are negligible compared to the mirror losses. The size of the mode in the cavity was about one half millimeter in full width, which is smaller than the separation of the points on the grid (1.3 mm). A number of aberrant points appear to be due to point defects or to dust particles adhering to the surface. While the forward mirror has degraded to $\Gamma_s \sim 4 \times 10^{-3}$ depending on the point which the mode touches, the rear mirror has also degraded to $\Gamma_n \sim 2 \times 10^{-3}$. Part, but not all of this difference is explainable by the length of time it takes to align the FEL cavity to the electron beam, during which time the rear mirror is not fully exposed to the radiation reflected from the forward mirror. The transverse dependance of the losses of the forward mirror resembles a symmetrical hump which is cut-off by the aperture of the mirror holder. This behaviour, which is even more obvious from the numbers than from the three dimensional plot, is probably due to a small ($\sim$ 2 mm) displacement of the cavity mode with respect to the geometric center of the mirror.

The results of the measurements made on a second set of mirrors appears in the third and fourth columns of table 6. This data was taken with the length-shifted cavity decay time technique. The curves of fig. 21 are selected from the sets of before- and after-exposure measurements, and were used in the calculation of the degradation rate in the fourth column. A first measurement at low beam energy shows no measurable degradation, whereas at high energy the degradation rate is enormous. The high degradation rate observed on this mirror set is neither due to the conditions of the exposure, which was well controlled, nor to the wavelength of operation. In fact, as we learned subsequent to the experiment, these mirrors were fabricated under conditions leading to the presence of a Ti impurity in the SiO_2 layer and a Si impurity in the TiO_2 layer. We attribute the poor performance of this mirror set to the impurities. This conclusion is supported by the independant observation of a high degradation rate of similar mirrors exposed to the plasma discharge of a HeNe laser.

The importance of the measurements in the last two columns of table 6 lies in the comparison between the two, and not in their absolute magnitude. The degradation rate is reduced by more than a factor of twenty by reducing the energy of the electron beam to 150 MeV. This occurs because of the concomitant reduction in the undulator magnetic field which is necessary to maintain the wavelength of the fundamental.

At high values of the undulator field parameter K, the high harmonics of the undulator radiation become extremely intense. Integrating over the spectrum of each harmonic, we find $/ \overline{} 27 \underline{} 7$ for the odd harmonics

$$I(\text{photons/sec/cm}^2/\text{ma}) = F(\gamma) \cdot G(K,n) \qquad (5)$$

where

$$F(\gamma) = \frac{Ne}{R^2 \hbar c} \overline{I}\gamma^2 = 1.02 \times 10^{10} \gamma^2 \text{ photons/sec/cm}^2/\text{ma}$$

$$G(K,n) = \frac{K^2 n}{(1 + \frac{K^2}{2})^2} \times \left[J_{\frac{n-1}{2}} \left(\frac{nK^2}{4+2K^2}\right) - J_{\frac{n+1}{2}} \left(\frac{nK^2}{4+2K^2}\right) \right]^2$$

and where N = 17 is the number of periods in the undulator, R = 275 cm is the mean distance from the undulator to the mirror surface, $\overline{I}$ the average electron current, n the harmonic number, and $K = eB\lambda_0/2\pi mc^2$ is the wiggler parameter. Fig. 24 shows the dependence on K of the harmonic spectrum for the case in which the energy of the electron beam is adjusted to maintain the wavelength of the fundamental constant at λ = 6328 Å. Note that these are universal curves. For a given K, the amplitude depends only on the energy, the number of periods in the undulator, and the distance from the source. The undulator period only affects the photon energy scale factor of the thorizontal axis. In a real undulator, the even harmonics will exist also

$\underline{/}$5, 10$\underline{/}$, due to magnetic field imperfections, and of course the spectrum of each harmonic line will depend on the phase space of the electron source.
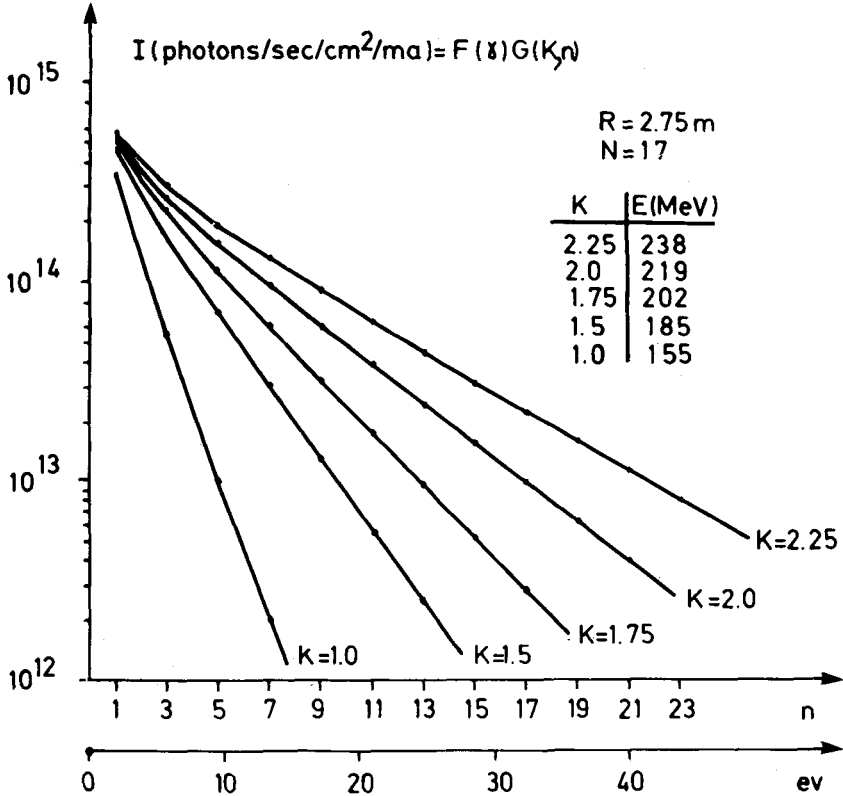

Figure 24 - Calculated values of the intensities of the odd harmonics of an ideal undulator are plotted for several values of the magnetic field parameter K. The electron energy is adjusted as shown so that the wavelength of the emitted radiation is constant. Under these conditions, NOEL emits 6328 Å or 1.9 eV photons in the fundamental.

It is clear that the reduction in harmonic intensity produced by the reduction in energy from 230 MeV to 150 MeV is enormous. As shown in table 6, the third harmonic drops by a factor of eight, while the fifth harmonic drops by a factor of thirty six. Since the degradation rate drops by more than a factor of twenty, we conclude that it is not the third harmonic which is primarily responsible for the degradation. All other harmonics are still possibilities as we have no lower bound on the low energy degradation rate. We plan in future experiments to measure the degradation rate for at least one intermediate energy in order to identify the wavelength range of the destructive radiation.

Discussion

There are two possible mechanisms which would be causing the UV degradation and
which are consistent with the data. UV radiation is known to form color centers
/ 28 / which absorb in the visible spectral region. This mechanism saturates at
a level which depends strongly on the material ; if we take 10 cm^{-1} as an order
of magnitude estimate of the saturated absorption coefficient of SiO$_2$, we find
for the mirrors that $\Gamma_{sat} \simeq 10^{-2} - 10^{-3}$. The second mechanism is photo-stimu-
lated desorption / 29 / of the oxygen from the TiO$_2$ layer. This process produces
a layer of sub-oxide which is strongly absorbing in the visible (Ti$_2$O$_3$ is blue-
black) and does not saturate. It is not known which of these two processes is
producing the degradation we observe on ACO. We expect to be able to answer the
question through a series of measurements at intermediate values of the undulator
magnetic field and electron energy since the photon energy thresholds of the
two processes are different.

A number of remedies are possible for the mirror degradation problem. As noted
above, the harmonic flux can be reduced by lowering the magnetic field of the un-
dulator. This solution, however, presents a number of disadvantages. First, the
adoption of such a design restraint significantly reduces the flexibility of the
free electron laser. The use of high field (K $\gtrsim$ 2) undulators permits tunability
of the output radiation without changing the energy of the electron beam and allows
the use of high energy machines to produce relatively long wavelength radiations.
The gain of a standard undulator is also optimized in the region K = 2. We conclude
that a considerable effort should be applied to a search for a solution to the
optics problem before considering such a design restraint on the undulator.

A second possibility lies in the use of a helical instead of a linear magnetic
field which would theoretically eliminate all harmonics on axis. Although the
problem has not yet been studied, it should be possible to reduce field errors
to a low enough level so that the harmonic amplitudes in a real device would be
small over the area of an optical mode aligned to the axis of the electron beam.
However, the helical configuration is technically more complex in its realization,
particularly if the magnetic field is to be adjustable. An additional problem for
a storage ring laser is the requirement for a large horizontal aperture during
injection. Again, the optimal solution would be to reduce or eliminate the degra-
dation of the optics rather than to encumber the FEL with a heavier load of tech-
nical requirements. And finally, neither of the undulator design changes is of
any value for the UV free electron laser where the fundamental line itself damages
the cavity optics.

Two types of solution to the optics problem spring immediately to mind : either one
can shield the mirrors from the damaging radiation with a material that does not
itself become damaged, or one can construct the mirrors out of materials which
resist irradiation.

Shielding is possible through the use of a Brewster window or through the direct
deposition of some UV absorber on the surface of the window. Whatever the shield
used, the additional losses introduced by this element at the laser frequency must
be maintained at a very low level. For the Orsay experiment, we are studying the
possibility of using a fused silica Brewster window inside the cavity as a VUV ab-
sorber, but it is not clear that it will be possible to reduce the absorption and
scatter losses to an acceptable level ($\sim 1 \times 10^{-4}$).

Of course, the most attractive solution of all would be to find mirror coating
materials which would not be subject to the degradation process. Although we plan
to experiment with different mirror materials and sputtered UV shields, the pos-
sibilities are much too numerous for us to make any systematic investigation with
the resources at our immediate disposal. On the other hand, the problem is very
real and immediate. All short-wavelength FEL systems will need high quality trans-
missive optics, whether they are multilayer reflection or anti-reflection coatings,

Brewster intracavity or output windows, or etalons. In view of the importance and universality of the problem it is our strong view that a systematic effort is needed to survey the UV damage resistance of optical materials.

VI - THE EXPERIMENTS WITH THE OPTICAL CAVITY

Alignment of the optical cavity

Fig. 25 is a sketch of the optical cavity mounted on the storage ring ACO, and also of the auxiliary optical set-up used for the alignment of the cavity and the study of the emission. As discussed in the previous section, the cavity mirrors have been mounted inside the storage ring vacuum to eliminate all possible intra-cavity losses.
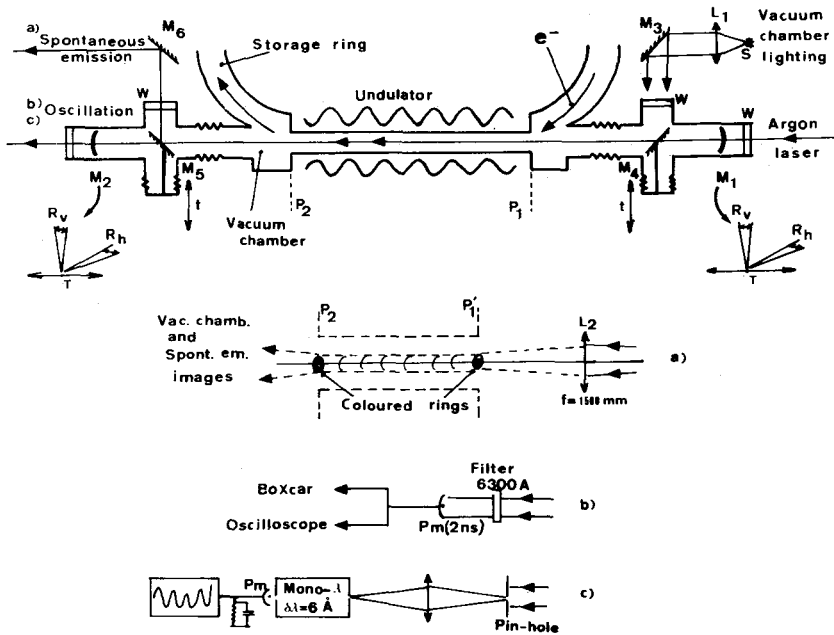

Figure 25 - The optical cavity and the optical set-up for alignment and the study of emission. M_1, M_2 : cavity mirrors ; R_V, R_H, T : rotations (vertical and horizontal) and longitudinal translation of cavity mirrors. M_3, M_4, M_5, M_6 : auxiliary mirrors for the alignment and the study of spontaneous emission ; t : translation of M_4 and M_5 (M_4, M_5 off : cavity, on : alignment of the cavity). W : silica or sapphire windows. P_1 and P_2 : entrance and exit planes of the undulator.

The length of cavity has been chosen in order to synchronize electron pulses and optical pulses with two bunches stored in the ring. For ACO, the repetitive rate being 27 MHz, the mirrors spacing is 5.5 m. The choice of cavity length was dictated by the presence of obstructing synchrotron and injection lines. If two bunches are stored in the ring, gain occurs on the stored optical pulse once per round trip. The only inconvenience of this arrangement is that the two bunches tend to oscillate longitudinally about their respective phase stable points (phase oscillations) so that the peak gain is reduced, on average, by an amount proportional to the phase oscillation amplitude.

Two optical structures were used. The first one, with mirrors of 6 m of radius of curvature, is almost a confocal cavity with a beam waist at 6328 Å of $w_0 \simeq 0.78$ mm which is approximately equal to the low current diameter of the electron beams (FWHM = 0.7 mm). The second structure is practically a concentric cavity with mirrors of radius 3 m and a beam waist $w_0 \simeq 0.41$ mm. These mirrors have an aperture of 16.5 mm and for both cavities diffraction losses are negligible even for high order modes. For example the diffraction losses of the confocal cavity are greater than 10^{-6} only for modes higher than $TEM_{18,18}$ or $TEM_{60,0}$. The geometrical structure of the spontaneous emission does not correspond exactly to the structure of the TEM_{00} mode. But since the cross section of the central part of the beam is approximately equal to the beam waist and the angular aperture is small (approximately 1.5 mrad for the wavelength where the gain has a maximum value), the emission is stored in only a few low order modes. Hence, the diffraction losses are negligible and the cavity losses are due only to the reflection coefficient of mirrors. For one round trip these losses are defined by $\Gamma = 1-R^2 \simeq 2p$, where p is the loss coefficient for one mirror. The adjustment of the cavity is performed in two steps. First, the centers of the mirrors need to be mechanically adjusted so that they fall on the magnetic axis of the undulator. This is done once with the aid of the undulator emission via an external laser. Then, during the experiments, the axis of the laser is aligned on the mirror centers, and both the electron beam and the mirror surfaces are aligned to the laser. In this way all alignments are referred to the axis of the undulator emission which is well defined in 17 periods as a result of our success in controlling the magnetic field errors /¯10_/. After following this procedure, we observe that a single symmetric beam is stored in the cavity, and fine mirror alignment can be made to optimize the stored power. The alignment of the system is an important problem made difficult by the cavity length (5.5 m) and its inaccessibility inside the vacuum system. We describe in detail the procedure we have developed to solve the alignment problem.

The initial alignment was performed with the aid of the auxiliary M_3 to M_6 mirrors (see fig. 25), in order to obtain an alignment of the electron trajectory on the magnetic axis of the undulator. This is necessary to avoid inhomogeneous broadening of the spectral lines due to off-axis effects /¯2_/. In our case the magnetic axis is very near the mechanical axis of the undulator vacuum chamber, and we use the latter for the preliminary alignment. The vacuum chamber is illuminated by a source S (a 40 W filament lamp) through the optical path M_3, M_4 (see fig. 25). With the aid of the M_5 and M_6 mirrors and the L_2 lens, an image of the vacuum chamber is formed simultaneously with an image of the spontaneous emission (see fig. 25a). Owing to the cylindrical symmetry of this emission, the center of the coloured rings can easily be located at the entrance and at the exit of the undulator. By using the storage ring correction coils the spontaneous emission can be centered on the mechanical axis with a precision of about 0.5 mm.

The alignment of M_1, M_2 cavity mirrors is performed by aligning the argon laser on the spontaneous emission with M_5 in the up position in order to avoid degradation of the mirrors. With the M_4 mirror down, the laser is sent through the cavity mirror M_1 and centered on the image of the spontaneous emission in order to define the cavity axis. The mechanical centring of M_1 and M_2 is then adjusted on the laser beam. This procedure ensures that the mirror centers lie on the magnetic axis of the undulator.

During the experiments, the mirrors are used as the reference point, the laser is centered on the mirrors, and the electron beam steering is adjusted so that the axis of the spontaneous emission coincides with the laser beam. Finally the mirrors are aligned on the laser as illustrated in fig. 26. With a mirror M' an auto-collimated beam is obtained at the rear of M_2 (see figure 26a). Then by using multiple reflexions between M' and M_2, a first alignment of M_2 can be easily achieved (figure 26 b) by vertical and horizontal rotations.
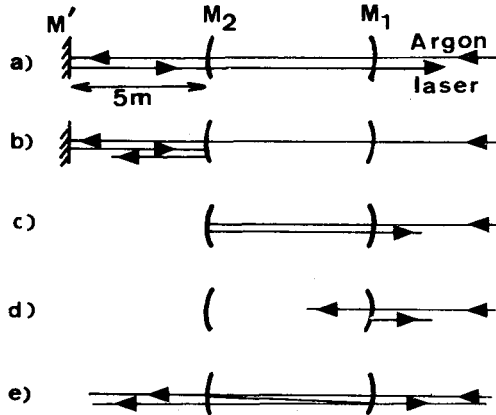
Figure 26

Alignment of the
optical cavity by
autocollimation of
an argon laser

This procedure yields an autocollimation of the reflected beam by M2 (fig. 26c).
The alignment of M_1 is also obtained by autocollimation (fig. 26d) and at this stage
a good superposition of multiple reflexions can be achieved on the right and left
part of the cavity.

Generally we obtain an excellent adjustment of the cavity with this procedure.
When the permanent magnet jaws are closed the spontaneous emission is stored at
the wavelength of maximum reflectivity and can be viewed in the central part of
the beam transmitted by the mirrors (see fig. 27). Its intensity is maximized
by a fine rotations of the mirrors. With this procedure the alignment is straight
forward and gives immediately a maximum of the stored intensity emission. This is
due to the fact that the axis of emission is very well defined, so that the cavity
is automatically centered on this axis.

The final step is the adjustment of the length of the cavity by a longitudinal
translation of mirrors in order to synchronize the optical and electronic pulses.
As discussed in section V, the time structure of the stored pulse has its minimum
width when the cavity length is synchronized with the half rotation time (fig.
28). Final length adjustment is performed using the integrated power output, and
while operating at a peak in the gain curve. A sharp peak is observed in the power
since the stored spontaneous emission amplified when the optical pulses remain syn-
chronized with the electron pulses. This amplification peak is typically 50 μ
in full width.

Measurements of amplification were made with the optical set up of fig. 25 c. A
0.4 mm pin-hole is set on the transmitted beam in order to let past only the central
part of the superposition of cavity modes which forms the stored beam. The amplifi-
cation is maximum in this central region. Then the beam is filtered by a monochro-
mator (bandwith of 6 Å) and the mean value of intensity is detected by a photomul-
tiplier followed by a low pass filter. The wavelength of the monochromator is set
on the maximum of the first derivative of the spontaneous emission spectra and the
length of cavity is tuned and detuned in order to display the amplification (red
side of spectra) or the absorption (blue side of spectra).

Enhancement factor

Measurements of amplification were made at two wavelengths (6300 and 5100 Å) with
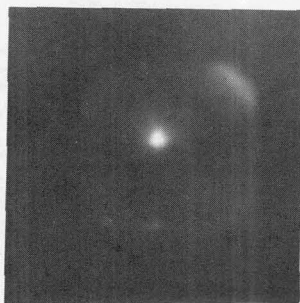the permanent magnet undulator (see section II) and with the optical klystron
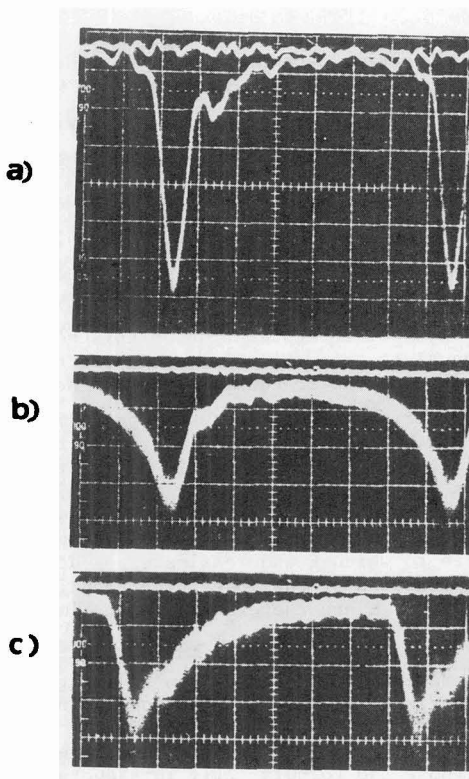
Figure 27 - Stored spontaneous emis-
sion when the cavity is tuned. The
central spot corresponds to 6300 Å
(maximum of reflectivity of mirrors).
The unstored green and blue second
order emission is also viewed as a
large blurring.

Figure 28 - Optical pulses for a
tuned (a) and detuned cavity
(b : 1 = - 3mm ; c : 1 = + 3 mm).
Time scale : 5 ns per division.

(see section IV). At the present time we have not obtained lasing action but we
have observed an enhancement of the stored spontaneous intensity as a result of the
gain process.

The observed enhancement factor E is defined by :

$$\frac{I_{tuned}}{I_{detuned}} = 1 + E \qquad (19)$$

For small amplifications, E is determined by the cavity losses and the gain per
pass (all saturation mechanisms being certainly negligible). The calculation of E
is complicated by the fact that the optical cavity stores many transverse modes with
low losses. For one mode E is related to the single pass gain g_n and the cavity los-
ses per round trip Γ_n of this n^{th} mode. If i_n is the intensity of the spontaneous
radiation emitted into the nth mode in one pass of the electron through the undula-
tor, then the steady state intensity in that mode is :

$$I_n = \frac{i_n}{P_n - g_n} \qquad (20)$$

When the length of the cavity is detuned by a distance large enough to displace the
optical pulse by one electron bunch length σ_1 in a few passes the gain effectively
drops to zero (this distance has been found experimentally to be on the order of
50 µ). For one mode the enhancement factor (19) is therefore :

$$e_n = \frac{g_n}{P_n - g_n} \qquad (21)$$

Here we have assumed that the gain g_n is independent of the intensities { i_n }

(no saturation mechanism) and that the phase of the spontaneous emission from pass to pass is uncorrelated so that we can add the intensities.

The total intensity stored in the cavity is then just $I = \sum_n I_n$ and the measured value of the enhancement factor is therefore :

$$E = \frac{\sum_n \frac{i_n}{P_n} \cdot e_n}{\sum_n \frac{i_n}{P_n}} \tag{22}$$

The physical interpretation of this result is clear : the net enhancement factor is equal to the weighted average of the individual mode enhancement factors, with a weighting factor equal to the intensity stored without amplification in that mode.

The experiments we report were performed with an overmoded cavity. The mode which is closest to threshold will provide the largest contribution to (22), but this contribution will necessarily be diluted by the averaging procedure which also takes into account the other modes which are farther from threshold. As a result, the measured enhancement factor is always smaller than the individual mode enhancement factor for the most interesting mode : the closest one to threshold. The degree to which E underestimates e_n depends on the distribution of gain and loss as a function of the mode number and is unknown for this system. The experimental values for E are therefore a lower limit to e_n for the most interesting mode.

Amplification with the permanent magnet undulator

Measurements of amplification at about 6300 Å were made by using an energy of 240 MeV, a magnetic field corresponding to K = 2.2 and a confocal cavity. Since the mode distribution is unknown, we cannot calculate the gain per mode from this data. An averaged gain $\bar{g}$ can be extracted from the measured values of E if we impose the formula (21). This average gain is probably a lower limit to the true gain for the mode closest to threshold.

Table 6 – Amplification and absorption measurements with the permanent magnet undulator and a set of 6250 Å mirrors. E = 240 MeV, K = 2.2

λ_{max} Spont. Em.	λ	Amplification E	Cavity losses Γ	Calculated $\bar{g}$ value	Ring current Γ
6220 Å $\{$	6390 Å	$+4.5 \overset{+}{-} 1$ %	18×10^{-4}	0.8×10^{-4}	56 mA
	6040 Å	$- 6$ %			
6100 Å $\{$	6170 Å	$+ 1.5$ %	26×10^{-4}	0.4×10^{-4}	105 mA
	5930 Å	$- 1.4$ %			
Cavity losses measured in air before irradiation			2×10^{-4}		
Gain value measured with an argon laser at 4880 Å				1.5×10^{-4}	

Table 6 gives the results of several measurements. The gain and the cavity losses were measured in the same conditions and practically simultaneously so that a good value of the averaged gain per round trip $\bar{g}$ can be calculated.

A small amplification was observed on the red side of spectra and also as expected a practically equal absorption on the blue side. The small value of amplification

is due primarily to the high value of cavity losses. As explained in section V these losses are due to the degradation of mirrors by irradiation. Amplification measurements were made after an irradiation of 5 hours (for λ_{max} = 6220 Å) and 10 hours for the second serie of experiments (λ_{max} = 6100 Å). A comparison with the cavity losses measured in air before irradiation shows an enhancement of these losses of one order of magnitude. With $\bar{g}$ = 8 x 10^{-5}, an enhancement factor E = 67 % would have been obtained in the absence of degradation. The second reason for such a small amplification is the low value of gain per pass $\bar{g}$. First the $\bar{g}$ value is lowered when the ring current increases. This effect is related to the evolution of electronic density versus the ring current (see section II) and to the increase in the number of modes stored in the cavity as the transverse area of the electron beam increase. We note also that during the first series of experiments (I = 56 mA) the sextupoles were in service on the storage ring, whereas during the second series they had broken down and could not be used. In the latter case both the density is lowered, and the transverse dimensions increase. Since the maximum current density is obtained for a current i ≃ 30 mA the effective gain $\bar{g}$ inside the cavity probably do not exceed 1 x 10^{-4}. This last value is smaller than the gain per pass, g = 2.2 x 10^{-4} deduced from the measurement with an argon laser and without cavity. It is likely this reduction is due to the modes of cavity, the mean value $\bar{g}$ being smaller than the gain for the TEM_{oo} mode. Some measurements of amplification were also made with a set of 5145 Å mirrors. In this case the amplification is practically equal to (or lower than) the sensitivity of measurements, and only an upper limit of E can be obtained (E < 1 %). This very bad result is mainly due to the higher value of mirror losses, $\Gamma \simeq 36.10^{-4}$.

Amplification with the optical klystron

The optical klystron used for these measurements is described in section IV. The vacuum chamber and the optical cavity are unchanged ; only the magnetic field generator is modified.

We used a new set of 6330 Å mirrors, and in order to prevent degradation of the mirrors by the high harmonics of the undulator radiation, we began our experiments at a lower magnetic field and therefore a lower energy (K = 0.89, E = 150 MeV). This operating point exhibits simultaneously the following three features :

- a fundamental wavelength in the red part of spectrum
- a maximum theoretical enhancement by a factor 5 of the gain of the optical klystron with respect to the gain obtained with the undulator (see section IV)
- a very low harmonics intensity in VUV and the X-ray range.

Working from the results of the amplification experiments with the undulator ($\bar{g} \simeq 1$ x 10^{-4}) a gain per pass of 5 x 10^{-4} was expected for the optical klystron. At low energy the real value of the average gain $\bar{g}$ would be reduced below this value if either the maximum current density drops or if the modulation of the klystron spectrum (see section IV) becomes significantly less than total. In fact, both of these phenomena occurs. The maximum current density drops at low energy due to the lower instabilities threshold of the electrons. The modulation is shown in fig. 29 which is a spectrum of the spontaneous emission transmitted by the cavity mirror. For those experiments the modulation rate defined by f = i_m/i_o can be far from 100 % and varies with the current stored in the ring.

The results of several measurements are reported in table 7. For the amplification measurements the wavelength (indicated by λ_G on fig. 29) was chosen in order to maximize the first derivative of the spectrum. A maximum amplification of 17 % was observed for the lowest value of the current stored in the ring.

No degradation of mirrors was observed during the experiments. Nevertheless the cavity losses are higher than the losses due to the in-air reflectivity of the mirrors as discussed in the previous section. If the cause of this vacuum-insertion degradation is identified and eliminated, the effects would be immediate and dramatic : under the same (rather unfavorable) circumstances, the enhancement

factor E would be 1.7.

Figure 29 -

Optical klystron :
spectrum of the spontaneous
emission transmitted by a
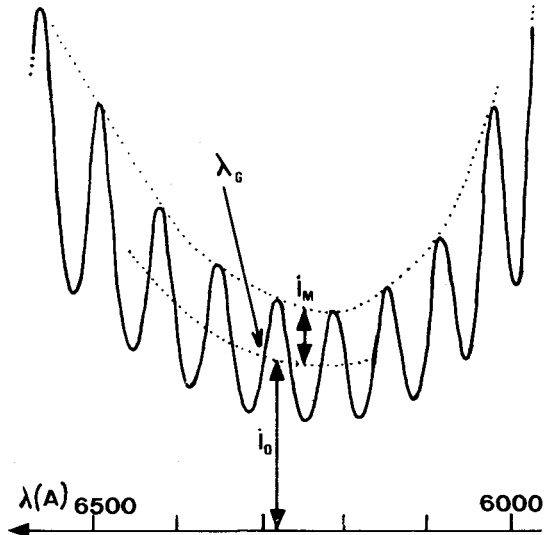cavity mirror. E = 150 MeV,
K = 0.9, ring current =
35 mA.

Table 7 - Amplification measurements for the optical klystron with a set of 6300 Å
mirrors from the batch Bε and an almost concentric cavity. E = 150 MeV, K ≃ 0.9

λ	Cavity losses Γ	Ring current i	Amplification E	Calculated $\bar{g}$ value (from eq. 22)	Modulation rate f	$\bar{g}$ 100 % (corrected for 100 % modulation)
6300 Å	7×10^{-4}	14 mA	17 %	1×10^{-4}	60 %	1.7×10^{-4}
6300 Å	7×10^{-4}	35 mA	13 %	0.8×10^{-4}	35 %	2.3×10^{-4}
6220 Å	6×10^{-4}	126 mA	12 %	0.65×10^{-4}	17 %	3.8×10^{-4}

When the current increases we observe a reduction of the modulation rate of the
spontaneous emission spectrum and simultaneously a reduction of gain. This effect
is mainly due to an enhancement of the energy spread and of the angular distribution
of velocities, which give an inhomogeneous broadening of spectral lines and then
reduce the modulation rate of the optical klystron / 20 /. Since the gain is pro-
portional to the first derivative of the spectrum / 14 /the theoretical gain value
is multiplied by f, and this reduction factor varies between 1.7 at low current and
6 for the highest value of current.

Taking into account the reduction due to the modulation rate, a corrected value of $\bar{g}$
can be calculated for an arbitrary 100 % modulation (last column of table 7), and
its variation with respect to the ring current is reported on fig. 30. Clearly this
curve shows a saturation of gain for high values of current. This effect is certain-
ly due to a saturation of the electronic density of the electron bunch. For ACO,
measurements of the size of the bunch show that the electronic density is propor-

Figure 30 -

Corrected value of
gain for 100 %
of modulation
rate
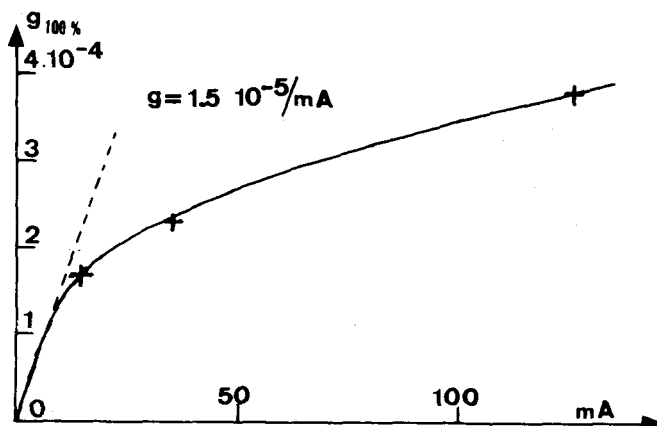
tional to the current only for small values of i, reaches a maximum value for
i = 30 mA and decreases slowly for higher currents (see fig. 11). The small dis-
crepancy between the curves of fig. 11 and 30 can be easily explained by the dif-
ference between both experiments : a measurement of electronic density and a mea-
surement of the enhancement factor for an optical klystron. The most important
feature is the saturation of electronic density and gain for a current higher than
30 mA. Then, the best choice of current is probably a rather low value of 15-30 mA
which gives a maximum of electronic density, without too much of inhomogeneous
broadening of spectra and degradation of mirrors.

For low values of current, fig. 30 shows also that the gain is proportional to the
current, the experimental value being g $\simeq$ 1.5 x 10^{-5}/mA. We can try to compare
this value with the expected value from the amplification measurements obtained with
the undulator. With an energy of 240 MeV and for the maximum of electronic density,
the gain of our undulator was g $\simeq$ 2 x 10^{-4} when measured with an argon laser, and
g $\simeq$ 1 x 10^{-4} when measured inside the cavity. Taking into account the variation of
electronic density (fig. 11) we can estimate for this undulator a gain at low
current 1 x 10^{-5}/mA < g < 2 x 10^{-5}/mA, so that the expected value of gain for our
optical klystron at 240 MeV was 5 x 10^{-5}/mA < g < 10 x 10^{-5}/mA. By using an energy
of 150 MeV, the experimental value is substantially smaller (nearly one order of
magnitude). Such a discrepancy can be explained also by the evolution of the elec-
tronic density with the energy of electron. An energy E = 150 MeV is an extreme
limit for ACO, and we have observed a large enhancement of the bunch sizes between
the nominal energy (240 MeV) and lower limit (150 MeV). So that the choice of a
low energy reduces the degradation of mirrors but also reduces the electronic den-
sity, and the net gain was practically unchanged. Then, the best choice of energy
is a compromise between both effects but, at the present time, we do not have any
results for intermediates energies.

From these experiments it is clear that severe reduction of gain observed in the
cavity can be due to several mechanisms :

- the irradiation by V-U-V or X-ray of mirrors (or Brewster' windows)
- the evolution of electronic density versus the ring current or the energy
- the inhomogeneous broadening of the optical klystron spectra mainly by the energy
  spread and the angular distribution of velocities.

Then in this work we have optimized a F.E.L. experiment which ultimate goal is to
reach the laser oscillation threshold. We have installed an permanent magnet undu-
lator and optical klystron and shown that they behave exactly as they were expected
to do. Also we have constructed a high vacuum optical cavity and used state of the

art mirrors. We have observed a substantial amplification of the stored spontaneous emission. However we have not reached the laser threshold although we are not far from it. We can consider that the optical parameters have been optimized as far as possible and that only the electron beam qualities and the mirrors degradation problems have to be improved. The electron bunch qualities can be improved in at least two ways :

- inserting a high-frequency cavity in the ring should reduce the bunch length of the bunches and then improve both the electronic density and the inhomogeneous broadening of the optical klystron line

- working with positrons will improve the bunch volume and then allow a greater electronic density at high current.

These improvements are planned for the near future at LURE.

The mirror degradation problem is also studied from several different points of view (different layers, inserting Brewster windows.... etc, see section V). We want only to point out that given the low optical gain attainable on most storage rings, this degradation problem is probably the frontier in the present and future F.E.L. work. In addition the accuracy of the degradation data obtained in the F.E.L. experiments may lead to great progress in the understanding of the multilayers coatings behavior under strong U.V. light exposure.

REFERENCES

/ 1 / BAZIN C., BILLARDON M., DEACON D.A.G., FARGE Y., ORTEGA J.M., PEROT J., PETROFF Y. and VELGHE M., J. Phys. Lettres, 41 (1980) 547
/ 2 / BILLARDON M. et al, to be published
/ 3 / DEACON D.A.G., MADEY J.M.J., ROBINSON K.E., BAZIN C., BILLARDON M., ELLEAUME P., FARGE Y., ORTEGA J.M., PETROFF Y. and VELGHE M., IEEE Trans. Nucl. Sci. NS-28-3142 (1981)
/ 4 / DEACON D.A.G., ROBINSON K., MADEY J.M.J., BAZIN C., BILLARDON M., ELLEAUME P., FARGE Y., ORTEGA J.M., PETROFF Y. and VELGHE M., Optics Communications 40, (1982), 373
/ 5 / BAZIN C., BILLARDON M., DEACON D.A.G., ELLEAUME P., FARGE Y., MADEY J.M.J., ORTEGA J.M., PETROFF Y., ROBINSON K. and VELGHE M., Phys. of quantum. El. Addison Wesley 8, chap. 4 (1982), 89
/ 6 / ORTEGA J.M.J., BAZIN C., DEACON D.A.G., DEPAUTEX C. and ELLEAUME P., Nucl. Inst. and Methods. To be published
/ 7 / HALBACH K., Nucl. Inst. and Methods, 169 (1980), 1
/ 8 / VINOKUROV N.A. and SKRINSKI A.N., Preprint INP 77, 59 Novosibirsk (1977) see also N.A. VINOKUROV, Proc Xth Intl. Cong. on High Energy Charge Particle Accelerators, Serpukhov, vol. 2 (1977) 454
/ 9 / ELLEAUME P., Physics of Quantum electronics, Addison-Wesley, 8, chapt. 5, (1982), 119
/ 10/ ORTEGA J.M., BAZIN C. and DEACON D.A.G., J. of Applied Physics, to be published
/ 11/ JEJCIC A. and POTAUX D., LAL Service "Anneaux de Collisions" Internal Report NI/05-82-Orsay (1982)
/ 12/ JACKSON J.D. "Classical electrodynamics" 2nd Ed. Section 14.5 Wiley and Sons NY (1975)

/ 13/ JEJCIC A. and POTAUX D., Service "Anneaux de Collisions" internal report
       NI/09-82 Orsay (1982)
/ 14/ MADEY J.M.J., Il Nuovo Cimento 50B (1979), 64
/ 15/ SANDS M. "The Physics of electron storage rings : an introduction", SLAC
       report n° 121, Stanford CA 94 305 (1965)
/ 16/ RENIERI A., IEEE Trans. Nucl. Sc. 26, (1979), 3827
/17 / ELIAS L.R., MADEY J.M.J. and SMITH T.I., Appl. Phys. 23 (1980), 9
/18 / PELLEGRINI C., IEEE Trans Nucl. Sci., NS-26, n° 3 (1979)
/19 / WILSON P.B., SERVRANSKX B., SABERSKY A.P., GAREYTE J., FISCHER G.E. and
       CHAC A.W., IEEE Trans. Nucl. Sci. NS-24 (1977), 1211
/20 / ELLEAUME P., elsewhere in this volume
/21 / DEACON D.A.G. and MADEY J.M.J., Applied Physics 19 (1979) 295
/22 / HERBELIN J.M., Mc KAY J.A., KWOH M.A., UEUNTEN R.H., UREVIG D.S., SPENCER D.J.
       and BENARD D.J., Applied Optics 19 (1980) 144
/23 / VINOKUROV N.A. and LITVINENKO U.N., "Method for measuring reflection coeffi-
       cients near unity" Preprint INP 79-24, Institute of Nuclear Physics 630090
       Novosibirsk USSR
/24 / OJAI Research, 11554 Ventura Ave, OJAI CA 39023

/25 / The OSA Handbook of optics (W.G. Driscoll and W. Vaughan ed., Mc Graw-Hill,
       NY 1978) gives values for the absorption and scattering losses in air. At
       5145 Å at sea level, aerosol scattering dominates all other loss mechanisms.
       The propagation distance to be expected in the laboratory depends on the
       concentration of dust, forepump vapor, and other aerosols in the air, but
       should clearly lie between the values quoted for clear air (37.6 km) and
       hazy air (1.2 km).
/26 / WONG G. and ANGELL C.A., Glass structure spectroscopy, Marcel Dekker Inc.
       NY (1976)
/27 / DEACON D.A.G. in proceeding of SRI-82. International conference on X-ray
       and V.U.V. synchrotron radiation instrumentation (Aug. 1982). To be published
       in Nuclear Instr. and Methods
/28 / SCHULMAN J.H. and COMPTON W.D., Color centers in solids, Pergamon Press,
       NY (1963)
/29 / KNOTEK M.L. and FEIBELMAN P.J., Surface Science 90 (1979), 78